https://doi.org/10.5194/essd-2020-100
Preprint. Discussion started: 2 June 2020

Open Access Earth System Science Data Discussions

A Six-year long (2013–2018) High-resolution Air Quality Reanalysis Dataset over China base on the assimilation of surface observations from CNEMC

Lei Kong[1,2], Xiao Tang[1,2], Jiang Zhu[1,2], Zifa Wang[1,2,3], Jianjun Li[4], Huangjian Wu[1,5], Qizhong Wu[6], Huansheng Chen[1], Lili Zhu[4], Wei Wang[4], Bing Liu[4], Qian Wang[7], Duohong Chen[8], Yuepeng Pan[1,2], Tao Song[1,2], Fei Li[1], Haitao Zheng[9], Guanglin Jia[10], Miaomiao Lu[11], Lin Wu[1,2], Gregory R. Carmichael[12]

[1]LAPC & ICCES, Institute of Atmospheric Physics, Chinese Academy of Sciences, Beijing, 100029, China
[2]College of Earth and Planetary Sciences, University of Chinese Academy of Sciences, Beijing, 100049, China
[3]Center for Excellence in Regional Atmospheric Environment, Institute of Urban Environment, Chinese Academy of Sciences, Xiamen 361021, China
[4]China National Environmental Monitoring Centre, Beijing, 100012, China
[5]Guanghua School of Management, Peking University, Beijing 100871, China
[6]College of Global Change and Earth System Science, Beijing Normal University, Beijing 100875, China
[7]Shanghai Environmental Monitoring Center, Shanghai, 200030, China
[8]State Environmental Protection Key Laboratory of Regional Air Quality Monitoring, Guangdong Environmental Monitoring Center, Guangzhou, 510308, China
[9]Key Lab of Environmental Optics and Technology, Anhui Institute of Optics and Fine Mechanics, Hefei Institutes of Physical Science, Chinese Academy of Sciences, Hefei, 230031, China
[10]School of Environment and Energy, South China University of Technology, University Town, Guangzhou 510006, China
[11]State Environmental Protection Key Laboratory of Urban Ambient Air Particulate Matter Pollution Prevention and Control, College of Environmental Science and Engineering, Nankai University, Tianjin 300350, China
[12]Center for Global and Regional Environmental Research, University of Iowa, Iowa City, IA, 52242, USA

Correspondence to: Xiao Tang (tangxiao@mail.iap.ac.cn) and Jiang Zhu (jzhu@mail.iap.ac.cn)

Abstract.

Air pollution in China has changed substantially since 2013, and the effects such changes bring to the human health and environment has been an increasingly hot topic in many scientific fields. Such studies, however, are often hindered by a lack of long-term air quality dataset in China of high accuracy and spatiotemporal resolutions. In this study, a six-year long high-resolution Chinese air quality reanalysis datasets (CAQRA) has been developed by assimilating over 1000 surface air quality monitoring sites from China National Environmental Monitoring Centre (CNEMC) using the ensemble Kalman filter (EnKF) and the Nested Air Quality Prediction Modeling System (NAQPMS). Surface fields of six conventional air pollutants in China, namely $PM_{2.5}$, PM_{10}, SO_2, NO_2, CO and O_3 for period 2013–2018, are provided at high spatial (15km×15km) and temporal (1 hour) resolutions. This paper aims to document this dataset by providing the detailed descriptions of the assimilation system and presenting the first validation results for the reanalysis dataset. A five-fold cross validation (CV) method was used to assess the quality of CAQRA. The CV results show that the CAQRA has excellent performances in reproducing the magnitude and variability of the surface air pollutants in China (CV R^2 = 0.52–0.81, CV RMSE = 0.54 mg/m^3 for CO and 16.4–39.3

https://doi.org/10.5194/essd-2020-100
Preprint. Discussion started: 2 June 2020

Open Access Earth System Science Data Discussions

μg/m^3 for other pollutants at the hourly scale). The interannual changes of the air quality in China were also well represented by CAQRA. Through the comparisons with the Copernicus Atmosphere Monitoring Service reanalysis (CAMSRA) produced by the European Centre for Medium-Range Weather Forecasts (ECWMF) based on assimilating satellite products, we show that the CAQRA has higher accuracy in representing the surface gaseous air pollutants in China due to the assimilation of surface observations. The finer horizontal resolution of CAQRA also makes it more suitable for the air quality studies in the regional scale. We further validate the $PM_{2.5}$ reanalysis dataset against the independent datasets from the U.S. Department of State Air Quality Monitoring Program over China, and the accuracy of $PM_{2.5}$ reanalysis was also compared to that of the satellite estimated $PM_{2.5}$ concentrations. The results indicate that the $PM_{2.5}$ reanalysis shows good agreement with the independent observations (R^2 = 0.74–0.86, RMSE =16.8–33.6 μg/m^3 in different cities) and its accuracy is higher than most satellite estimates. This dataset would be the first high-resolution air quality reanalysis dataset in China that can simultaneously provide the surface concentrations of six conventional air pollutants in China, which should be of great value for many studies, such as the assessment of health impacts of air pollution, investigation of the changes of air quality in China and providing training data for the statistical or AI (Artificial Intelligence) based forecast. The whole datasets are freely available at: https://doi.org/10.11922/sciencedb.00053 (Tang et al., 2020a), and a teaser product which contains the monthly and annual mean of the CAQRA has also been released at https://doi.org/10.11922/sciencedb.00092 (Tang et al., 2020b) to facilitate the potential users to download and to evaluate the improvement of CAQRA.

1 Introduction

Air pollution is a critical environmental issue that humanity is facing, which adversely affects the human health and intimately connects to the climate change (von Schneidemesser et al., 2015). Exposure to ambient air pollution has been confirmed by many epidemiological studies to be a leading contributor to the global disease burden, which increases both morbidity and mortality (Cohen et al., 2017).

China, as the largest developing country, has achieved great economic development since 1980s. Such large economic expansion, however, is accompanied by a dramatic increase in emissions of air pollutants, leading to severe air pollution in China (Kan et al., 2012). To deal with the increasingly severe air pollution, from 2012 the Chinese government began to establish the nationwide ground-based air quality monitoring network (Fig. 1) to monitor the surface concentrations of six conventional air pollutants in China, namely $PM_{2.5}$, PM_{10}, SO_2, NO_2, CO and O_3. Since then, this network has consistently provided valuable observation data for both the operational use and scientific research, which plays an irreplaceable role in the understanding of air pollution in China. In addition, a series of aggressive control measures has been conducted in China to reduce the emissions of air pollutants. From 2013 to 2017, the Chinese government has implemented the Action Plan on the Prevention and Control of Air pollution, leading to a remarkable decrease in emissions of major air pollutants. According to the estimates of Zheng et al., 2018b, China's anthropogenic emissions decreased by 59% for SO_2, 21% for NO_x, 23% for CO,

https://doi.org/10.5194/essd-2020-100
Preprint. Discussion started: 2 June 2020

36% for PM_{10} and 35% for $PM_{2.5}$. Concurrently, the air quality in China has changed dramatically over the past six years (Silver et al., 2018; Zheng et al., 2017). Such large changes in the Chinese air quality and the effects they brought to the human health and environment has become an increasingly hot topic in many scientific fields(e.g. Xue et al., 2019; Zheng et al., 2017). Although the ground-based observations could provide valuable information on the spatial and temporal distributions of the air pollutants in China, the air quality monitoring sites are sparse with low spatial resolution and are unevenly distributed. As a result, such studies are often hindered by a lack of long-term air quality datasets in China of high accuracy and spatiotemporal resolutions for these years, which is urgently needed to provide a scientific basis for these studies.

Satellite observations have advantages of high spatial coverage and are widely used in the monitor of air pollution over wide domains. A series of satellite retrievals related to the air quality have been developed over the past two decades, such as the NO_2, SO_2 and O_3 observations from OMI (Ozone Monitoring Instrument; Levelt et al., 2006), CO observations from MOPITT (Measurement of Pollution in the Troposphere; Deeter et al., 2003) and AOD observations from MODIS (Moderate Resolution Imaging Spectroradiometer; Barnes et al., 1998). However, satellite measurements can only provide the column information on the air pollutants. Techniques that relate the surface concentrations to the satellite column measurements are thus required to estimate the surface concentrations of air pollutants. For example, various methods have been developed to estimate the surface $PM_{2.5}$ concentrations based on the satellite-derived AOD, including chemical transport models(van Donkelaar et al., 2016; van Donkelaar et al., 2010), advanced statistical methods(Ma et al., 2014; Ma et al., 2016; Xue et al., 2019; Zou et al., 2017) and semi-empirical models(Lin et al., 2015; Lin et al., 2018), which have been proven to be an effective way to monitor the wide-coverage $PM_{2.5}$ distributions in a good accuracy (Chu et al., 2016; Shin et al., 2019). However, challenges still remain in the satellite-estimated concentrations due to the missing values related to cloud contamination, uncertainties in satellite measurement and retrieval algorithms, and the difficulties in modeling the complex relationship between the surface concentrations and satellite measurements (Shin et al., 2019; van Donkelaar et al., 2016; Xue et al., 2019). In addition, most of previous satellite estimates of surface concentrations were limited to specific regions and time period and has a daily or even longer temporal resolutions due to the issues with data availability (e.g. incomplete coverage of AOD-based estimates), which limits their usage in the studies at finer scale, such as the assessment of acute health effects of air quality. To our best knowledge, a nationwide long-term estimate of surface concentrations of all conventional air pollutants in China at the hourly scale has still not been reported by previous satellite estimates.

A long-term air quality reanalysis of criteria air pollutants would provide constrained estimates of concentrations at all locations and times, which optimally combines the accuracy of observations and the physical information and spatial continuity of the chemistry transport models (CTMs) through advanced data assimilation techniques. Reanalysis is a uniform, continuous and state-of-science best-estimate data product, which has been used by a vast number of research communities. For example, several long-term meteorology reanalysis has been developed by the weather centres from different regions/countries, such as ERA-Interim reanalysis by European Centre for Medium Range Weather Forecasts (ECMWF; Dee et al., 2011), NCEP/NCAR Reanalysis by National Centers for Environmental Protection (NCEP; Saha et al., 2010), MERRA-2 by NASA Global Modeling and Assimilation Office (NASA-GMAO; Rienecker et al., 2011), JRA-55 by Japan Meteorological Agency

https://doi.org/10.5194/essd-2020-100
Preprint. Discussion started: 2 June 2020

(Kobayashi et al., 2015) and CRA-40 by China Meteorological Administration. The use of data assimilation in reanalysis of atmospheric chemistry is more recent, and some reanalysis datasets for atmospheric compositions have been produced over the past decades, for example the MACC, CIRA, CAMS reanalysis by ECWMF (Flemming et al., 2017; Inness et al., 2019; Inness et al., 2013), MERRA-2 aerosol reanalysis by NASA-GMAO (Randles et al., 2017), tropospheric chemistry reanalysis (TCR) for years 2005–2012 by Miyazaki et al., 2015 and its latest version TCR-2 (Miyazaki et al., 2020), the global reanalysis of carbon monoxide by Gaubert, B., 2016, multi-sensor reanalysis of total ozone for years 1970–2012 by van der A et al., 2015 and Japanese Reanalysis for Aerosol (JRAero) for years 2011–2015 by Yumimoto et al., 2017. These reanalysis datasets have promoted our understanding of the atmospheric compositions and are also helpful for the air quality researches. However, these are all global datasets having coarse horizonal resolutions (> 50km), which may be insufficient for capturing the high spatial variability of the air pollutants at the regional scale. In addition, some of these reanalysis datasets only provided the air quality data priori to year 2012 and only focused on specific species, for example the aerosol and ozone reanalysis. To our best knowledge, there is still no high-resolution air quality reanalysis dataset in China for recent years when China's air quality changed dramatically.

In view of these discrepancies, in this study we will develop a high-resolution regional air quality reanalysis dataset over China for years 2013–2018 (will be extended in the future by adding one year each year) by assimilating over 1000 surface observation sites from China National Environmental Monitoring Centre (CNEMC) in a post processing mode using our own developed chemical data assimilation system (ChemDAS). The developed reanalysis dataset will help fill the gaps in the high resolution air quality dataset in China by providing the surface concentration fields of all six conventional air pollutants in China at high spatial (15km×15km) and temporal (hourly) resolutions. This dataset would be the first high-resolution air quality reanalysis dataset in China that can simultaneously provide the surface concentrations of six conventional air pollutants in China, which should be of great value in (1) retrospective analysis of air quality in China, (2) assessment of health and environmental impacts of air pollution in fine scales; (3) model evaluation and satellite calibration, and (4) provide basic training dataset for statistical or AI (Artificial intelligence) based forecast.

2 Description of chemical data assimilation system (ChemDAS)

The Chinese air quality reanalysis dataset was produced by the chemical data assimilation system developed by the Institute of Atmospheric Physics, Chinese Academy of Sciences (Tang et al., 2011). This system consists of (i) a three-dimensional chemical transport model (CTM) called Nested Air Quality Prediction Modeling System (NAQPMS) developed by Wang et al., 2000, (ii) an ensemble Kalman filter (EnKF) assimilation algorithm, and (iii) surface observations from CNEMC with an automatic outlier detection method (Wu et al., 2018). We used an offline analysis scheme in this study since there is no previous experiences for the online run of chemical data assimilation system under such high horizontal resolution. The lessons learned from the offline analysis would feed into the future implementation of online analysis. In the offline analysis scheme, a free run of ensemble simulation was first conducted, and then the observations were assimilated using the

https://doi.org/10.5194/essd-2020-100
Preprint. Discussion started: 2 June 2020


Open Access Earth System Science Data Discussions

EnKF and the results of ensemble simulation. The similar offline analysis scheme has also been used in previous reanalysis studies, such as Candiani et al., 2013 and Kumar et al., 2012. Detailed descriptions of the ensemble simulation, observations and the data assimilation algorithm used in this study are presented below.

2.1 Air Pollution Prediction model

Reanalysis focuses on the retrospective analysis over long time periods. It uses the same air pollution model used to produce forecasts, but the meteorology fields used to drive the CTM are more accurate as they use simulated fields as opposed to forecasted fields used to forecast air quality. In addition, reanalysis using a more comprehensive set of observations to provide constraints. The same NAQPMS model used as an operational forecast model, which has been used in previous assimilation studies(Tang et al., 2011; Tang et al., 2013), has been used for the reanalysis in this study. The model is driven by the hourly meteorological fields produced by the Weather Research and Forecasting Model (WRF; Skamarock, 2008). The gas phase chemistry is simulated with the Carbon-Bond Mechanism Z (CBM-Z) developed by Zaveri and Peters, 1999. Aqueous-phase chemistry and wet deposition are simulated based on the Regional Acid Deposition Model (RADM) mechanism in the Community Multi-scale Air Quality (CMAQ) version 4.6. For aerosol processes, the thermodynamic model ISORROPIA 1.7 (Nenes et al., 1998) is used for the simulations of inorganic atmospheric aerosols. Six secondary organic aerosols (SOA) were explicitly treated in NAQPMS based on Li et al., 2011. To simulate the interactions between the particles and gases, 28 heterogeneous reactions on sulfate, soot, dust and sea salt particles were included based on the previous studies (Li et al., 2015; Li et al., 2012). Size-resolved mineral dust emission is calculated online as a function of relative humidity, friction velocities, mineral particle size distribution and surface roughness (Li et al., 2012). Sea-salt emission is calculated using a scheme of Athanasopoulou et al., 2008. Dry deposition of gases and aerosols is modelled based on the scheme of Wesely, 1989, and the advection is simulated with an accurate mass-conservative algorithm from Walcek and Aleksic, 1998.

Figure 1 shows the modeling domain of this study, which covers the most parts of East Asia with a fine horizontal resolution of 15km. The vertical coordinate system is set as 20 terrain-following levels with the model top up to 20000 m and the first layer about 50m. Nine vertical layers were set within the 2km closet to the surface to better characterise the vertical mixings within the boundary layers. Emissions of air pollutants used in this study included monthly anthropogenic emissions from HTAP_v2.2 emission inventory at base year of 2010 (Janssens-Maenhout et al., 2015), biomass burning emissions form Global Fire Emissions Data base (GFED) version 4 (Randerson et al., 2017; van der Werf et al., 2010), biogenic volatile organic compounds (BVOC) emissions from MEGAN-MACC (Sindelarova et al., 2014), marine VOCs emissions from POET database (Granier et al., 2005), soil NO_x emissions from Regional Emission inventory in Asia (Yan et al., 2003) and the lightning NOx emissions from Price et al., 1997. The clean initial conditions were used in the air quality simulation with a two-week free run of NAQPMS as a spin-up time. Top and boundary conditions were provided by the global chemical transport model MOZART (The Model for Ozone and Related Chemical Tracers; Brasseur et al., 1998; Hauglustaine et al., 1998) and the meteorology fields were provided by the WRF model. In each day's meteorology simulation, a 36-h free run of WRF was conducted with the first 12-h simulation as a spin-up run and the remaining 24-h to provide the meteorology inputs for

https://doi.org/10.5194/essd-2020-100
Preprint. Discussion started: 2 June 2020


Open Access Earth System Science Data Discussions

NAQPMS. Initial and boundary conditions for the meteorology simulation were provided by the National Center for Atmospheric Research/National Center for Environment Prediction (NCAR/NCEP) 1° × 1° reanalysis data.

Previous studies have shown that the emissions are a major contributor to the prediction uncertainty of air quality (Carmichael et al., 2008; Hanna et al., 1998; Li et al., 2017). Uncertainties of emission inventories were thus considered in the ensemble simulation which was driven by an ensemble of perturbed emissions ($E_i; i = 1, 2, \cdots, N_{ens}$). The emissions were perturbed based on their error probability distribution functions (pdf), which were assumed to be Gaussian distribution in this study. Table 1 lists the perturbed species considered in this study as well as their corresponding emission uncertainties obtained from previous studies. An isotropic correlation model was assumed in the covariance of the emission errors, which was written as:

$$\rho(i,j) = exp\left\{-\frac{1}{2}\left[\frac{h(i,j)}{l}\right]^2\right\} \quad (1)$$

where $\rho(i,j)$ represents the correlation between grid i and j, $h(i,j)$ represents the distance between these two points and l represents the decorrelation length, which was specified as 150km in this study. The ensemble of emissions was simply obtained by multiplying the base emissions with a perturbation factor $\boldsymbol{\beta}$ as shown in Eq. (2):

$$\boldsymbol{E_i} = \boldsymbol{E} \circ \boldsymbol{\beta_i} \quad (2)$$

where $\boldsymbol{E}$ represents the vector of base emissions and ∘ denotes the schur product. According to the pdf of emission errors, $\boldsymbol{\beta}$ follows the same Gaussian distribution with the emission errors except that its mean equals to 1. The performance of EnKF is strongly related to the ensemble size. In this study, the ensemble size was chosen as 50 to maintain a balance between the computational cost and the filter performance. Based on the method of Evensen, 1994, fifty smooth pseudo random perturbation fields for $\boldsymbol{\beta}$ were generated for each perturbed species. The emission perturbations were kept independent from each other to prevent the pseudo correlation among different species.

2.2 Observations

Surface observations of hourly ambient $PM_{2.5}$, PM_{10}, SO_2, NO_2, CO and O_3 concentrations from the CNEMC were used in this study. The number of observation sites was about 510 in 2013 and increased to 1436 in 2015. Real-time observations of these six air pollutants at each monitoring sites are routinely uploaded to the CNEMC and released to the public (available at http://www.cnemc.cn/, last access: 17 Apr, 2020) with an hour interval.

The quality control of observations is critical for the data assimilation since outliers of observations can exert catastrophic impacts on the performance of assimilation. To deal with it, a fully automatic outlier detection method was developed to filter out the outliers of observations (Wu et al., 2018). An automatic way of outlier detection is very important in the chemical data assimilation since there is large amount of observation data from multiple species. Four types of outliers characterised by the temporal and spatial inconsistency, instrument-induced low variances, periodic calibration exceptions and less PM_{10} than $PM_{2.5}$

https://doi.org/10.5194/essd-2020-100
Preprint. Discussion started: 2 June 2020


Open Access Earth System Science Data Discussions

in concentrations were detected and removed before the assimilation. More details about the outlier detection method are available in Wu et al., 2018.

A proper estimate of observation error is important for the performance of filter since the observation and background error determine the relative weights of the observation and background value on the analysis. The observation error includes the measurement error and representativeness error. For each species, the measurement error was given by their instruments, that is 5% for $PM_{2.5}$ and PM_{10}, 2% for SO_2, NO_2 and CO, and 4% for O_3 according to the officially released documents of the Chinese Ministry of Ecology and Environmental Protection (HJ 193–2013 and HJ 654–2013, available at http://www.cnemc.cn/jcgf/dqhj/, last access: 17 Apr, 2020). The representativeness error arises from the different spatial scales that the discrete observation data and model simulation represent, which was estimated based on the previous study by Li et al., 2019 who estimated the representativeness errors under the 30km horizontal resolution. We extended their estimates to the 15km model resolution in this study according to the method of Elbern et al., 2007 which is formulated by:

$$r_{repr} = \sqrt{\frac{\Delta x}{L_{repr}}} \times \epsilon^{abs} \quad (3)$$

where r_{repr} represents the representativeness error, Δx represents the model resolution, L_{repr} represents the characteristic representativeness length of the observation site and ϵ^{abs} represents the error characteristic parameters related to different species. Most of the observation sites in CNEMN are city sites with L_{repr} about 2km according to Elbern et al., 2007. Using the previous estimated representativeness errors under the 30km model resolution, the ϵ^{abs} could be estimated simply by a transformation of Eq. (3). The representativeness errors under other model resolutions were then estimated by specifying the Δx in Eq. (3).

2.3 Data assimilation algorithm

We used a variation of EnKF approach, i.e., a local ensemble transform Kalman filter (LETKF; Hunt et al., 2007), to assimilate observations into model state. Like any other EnKF implementation the ETKF uses a stochastic ensemble of model realizations to represent the background error covariance matrix, while it solves the analysis equations in the space spanned by the ensemble perturbations (Bishop and Toth, 1999). It is a kind of deterministic filter that does not need to perturb the observations which avoids the introduction of additional sampling errors. The LETKF is a local implementation of ETKF which calculates the analysis grid by grid by only using the observations from the region surrounding this analysis grid. By performing the analysis locally, there is no need to represent the full error space of the global state. Instead, the ensemble perturbations of limited ensemble size only need to represent a low-dimensional error space within the local region, which well addresses the rank problem of EnKF resulting from the limited ensemble size. In addition, the long-distance spurious correlation can also be supressed by the local implementation. The formulation of LETKF in a local region can be written as

$$\overline{\boldsymbol{x}^{\boldsymbol{a}}} = \overline{\boldsymbol{x}^{\boldsymbol{b}}} + \mathbf{X}^{\mathbf{b}}\overline{\boldsymbol{w}}^{\boldsymbol{a}} \quad (4)$$

https://doi.org/10.5194/essd-2020-100
Preprint. Discussion started: 2 June 2020

Open Access Earth System Science Data Discussions

$$\bar{\boldsymbol{w}}^{\boldsymbol{a}} = \tilde{\mathbf{P}}^{\mathbf{a}}\left(\mathbf{H}\mathbf{X}^{\mathbf{b}}\right)^{\mathbf{T}}\mathbf{R}^{-1}(\boldsymbol{y}^{\boldsymbol{o}} - \mathbf{H}\overline{\boldsymbol{x}^{\boldsymbol{b}}}) \quad (5)$$

$$\tilde{\mathbf{P}}^{\mathbf{a}} = \left[\frac{(N_{ens}-1)\mathbf{I}}{1+\lambda} + \left(\mathbf{H}\mathbf{X}^{\mathbf{b}}\right)^{\mathbf{T}}\mathbf{R}^{-1}\left(\mathbf{H}\mathbf{X}^{\mathbf{b}}\right)\right]^{-1} \quad (6)$$

$$\overline{\boldsymbol{x}^{\boldsymbol{b}}} = \frac{1}{N_{ens}}\sum_{i=1}^{N_{ens}}\boldsymbol{x}_{\boldsymbol{i}}^{\boldsymbol{b}}\,;\mathbf{X}_{\mathbf{i}}^{\mathbf{b}} = \frac{\mathbf{1}}{\sqrt{N-1}}\left(\boldsymbol{x}_{\boldsymbol{i}}^{\boldsymbol{b}} - \overline{\boldsymbol{x}^{\boldsymbol{b}}}\right) \quad (7)$$

where $\overline{\boldsymbol{x}^{\boldsymbol{a}}}$ represents the analysis state and $\overline{\boldsymbol{x}^{\boldsymbol{b}}}$ represents the background state. $\mathbf{X}^{\mathbf{b}}$ represents the background perturbations calculated by using the results of ensemble simulation and $\bar{\boldsymbol{w}}^{\boldsymbol{a}}$ is the analysis in the ensemble space spanned by $\mathbf{X}^{\mathbf{b}}$. $\tilde{\mathbf{P}}^{\mathbf{a}}$ represents the analysis error covariance in the ensemble space with a dimension of $N_{ens} \times N_{ens}$. $\mathbf{y}^{\mathbf{o}}$ denotes the vector of observations used in the analysis of this grid and $\mathbf{R}$ is the observation error covariance matrix. $\mathbf{H}$ represents the linear observational operator that maps the model space to the observation space. The scalar λ in Eq. (6) denotes the inflation factor for the background covariance matrix which was estimated by an algorithm proposed by Wang and Bishop, 2003:

$$\lambda = \frac{\left(\mathbf{R}^{-1/2}\boldsymbol{d}\right)^{\mathrm{T}}\mathbf{R}^{-1/2}\boldsymbol{d} - p}{trace\left\{\mathbf{R}^{-1/2}\mathbf{H}\mathbf{P}^{\boldsymbol{b}}\left(\mathbf{R}^{-1/2}\mathbf{H}\right)^{\mathrm{T}}\right\}} \quad (8)$$

$$\boldsymbol{d} = \boldsymbol{y}^{\boldsymbol{o}} - \mathbf{H}\overline{\boldsymbol{x}^{\boldsymbol{b}}} \quad (9)$$

$$\mathbf{P}^{\boldsymbol{b}} = \mathbf{X}^{\mathbf{b}}\left(\mathbf{X}^{\mathbf{b}}\right)^{\mathbf{T}} \quad (10)$$

where $\boldsymbol{d}$ represents the observation-minus-forecast residuals, p represents the number of observations, and $\mathbf{P}^{\boldsymbol{b}}$ represents the ensemble estimated background error covariance matrix. The inflation is necessary for the ensemble-based assimilation algorithm since the ensemble estimated background error covariance is very likely to underestimate the true background error covariance due to the limited ensemble size and the existence of model error (Liang et al., 2012). Without any treatment to prevent the underestimation of background error covariance, the model forecast would be overconfident and eventually result in filter divergence.

To prevent the spurious correlation between non or weakly related variables, each air pollutant is assimilated independently by only using the observations of this pollutant. Figure 2 illustrates the local scheme we used in the assimilation, where the plus signs and dots respectively denote the centre of model grids and the location of observation sites. For each model grid, only the observation sites located within a $(2l+1)$ by $(2l+1)$ rectangular area centred at this model grid are used in the analysis of this model grid. The cut-off radius l was chosen as 12 model grids, approximate to 180 km under the 15km horizontal resolutions. The use of cut-off radius, however, could lead to discontinuities in the analysis when an observation "enters" or "leaves" the local domain as one moves from one model grid to another (Sakov and Bertino, 2011). In order to increase the smoothness of the analysis state, following Hunt et al., 2007, we artificially reduced the impact of the observations close to the boundary of local domain by multiplying the entries in $\mathbf{R}^{-1}$ by a factor that decays from one to zero as the distance of the observation from the central model grid increases. The decay factors used in this study were calculated by

$$\rho(i) = exp\left\{-\frac{h(i)^2}{2L^2}\right\} \quad (11)$$

https://doi.org/10.5194/essd-2020-100
Preprint. Discussion started: 2 June 2020

where $\rho(i)$ denotes the decay factor for the observation i, $h(i)$ is the distance between the observation i and the central model grid point, and L is the decorrelation length that was chosen as 80 km, smaller than the cut-off radius, to increase the smoothness of the analysis state. Typically, only the state of the central model grid needs to be updated and used to construct the global analysis field. However, the experiences show that there is still observable discontinuity seen in the analysis over some regions. To deal with it, following the method of Ott et al., 2004, we simultaneously updated the state of a small patch (l =1) around the central model grid (updated region in Fig. 2) in each local analysis step. The final analysis of one model grid is then obtained by a weighted mean of all the values that result from the analysis of the patches containing this model grid. A weighted mean is necessary since the analysis of different patches uses different decay factors for the observation error. The weight of each analysis value for model grid i is calculated by Eq. (9):

$$W_{i,j} = \frac{\exp\left(-\frac{h(i,j)^2}{L^2}\right)}{\sum_{j=1}^{m} \exp\left(-\frac{h(i,j)^2}{L^2}\right)} \quad (9)$$

where $h(i,j)$ denotes the distance of the model grid i from the central model grid of the patch that generated jth analysis value of this grid, m represents the number of patch that containing this model grid and L is the decorrelation length which was chosen as 80km in this study.

4 Results

This section presents the fields from the Chinese air quality reanalysis dataset (CAQRA) and compares them with observations. It aims to provides a brief introduction to the CAQRA and gives a first assessment of the quality of this dataset. The cross validation method was used in the assessment of CAQRA, in which a proportion of observation data is withheld from the data assimilation and used as a validation dataset. We conducted five cross validation experiments by randomly dividing the observation sites from CNEMN into five groups (20% observation sites for each group). In each experiment, the analysis was performed with one group's observation data left out in the assimilation. The analysis results at validation sites, i.e., the observation sites that are not used in the assimilation, were then collected and used to validate the assimilation. For convenience, the analysis results at validation sites from the five cross validation experiments were combined together and composed of a validation dataset containing all observations sites (cross validation run). This dataset was then evaluated against the observations to assess the qualities of CAQRA. Besides, the independent observations of $PM_{2.5}$ from the U.S. Department of State Air Quality Monitoring Program over China were also used in the assessment of $PM_{2.5}$ reanalysis field. The qualities of CAQRA was assessed at different spatial and temporal scales to better understand the qualities of CAQRA. Also shown are the validation results of the ensemble mean of the simulations without assimilation (base simulation) to highlight the impacts of assimilation.

https://doi.org/10.5194/essd-2020-100
Preprint. Discussion started: 2 June 2020


Open Access Earth System Science Data Discussions

4.1 PM

4.1.1 Spatial distributions of PM reanalysis over China

We first present the reanalysis fields of the PM concentrations ($PM_{2.5}$ and PM_{10}) in China. Figure 3 shows the six-year mean (2013–2018) spatial distributions of the $PM_{2.5}$ concentrations in China from CAQRA, base simulation and observations. The CAQRA presents a continuous map of the $PM_{2.5}$ concentrations in China, and well reproduced the observed magnitude of $PM_{2.5}$ concentrations in China. The largest $PM_{2.5}$ concentrations were located in the NCP region due to the intensive industrial activities and the associated high emissions of $PM_{2.5}$ and its precursors (Qi et al., 2017). Higher $PM_{2.5}$ concentrations were also found in the SE region where the $PM_{2.5}$ concentrations are both influenced by the local emissions and the long range transport of the air pollutants from north China (Lu et al., 2017). In the NW region, besides the hotspots of $PM_{2.5}$ concentrations in big cities, high $PM_{2.5}$ concentrations were also obvious in the Taklimakan Desert due to the influences of dust emissions. The observed magnitude and spatial variability of PM_{10} concentrations were also well represented by the PM_{10} reanalysis. In general, the spatial distributions of PM_{10} reanalysis were similar to that of the $PM_{2.5}$ reanalysis except in the Gansu and Ningxia provinces where there were high PM_{10} concentrations but relatively low $PM_{2.5}$ concentrations. This would be related to the large contributions of dust emissions in these areas. The base simulation significantly overestimated the $PM_{2.5}$ and PM_{10} concentrations in China, especially in south China. This would be due to the systematic biases in the emission inventory (Kong et al., 2019) and also due to that the negative trends of the PM and its precursors' emissions were not considered in our simulation. In addition, the hotspots of $PM_{2.5}$ concentrations in the NW region and Tibet Plateau also failed to be captured by the base simulation possibly due to the absence of the activity data in these remote regions.

The seasonal maps of $PM_{2.5}$ and PM_{10} concentrations are shown in Figs. S1–2 in the Supplement, which shows significant seasonal variations. Both the $PM_{2.5}$ and PM_{10} concentrations show maximum values in winter in most regions of China due to the increased anthropogenic emissions related to enhanced power generation, industrial activities and the fossil fuel burnings for heating (Li et al., 2017). The unfavourable meteorological conditions with stable boundary condition would also contribute to the high PM concentrations in winter. In contrast, due to the lower emission rate and more intense mixing processes, the PM concentrations were lowest during summer. The PM concentrations in Taklimakan Desert exhibit a different seasonality with PM concentrations highest in spring and lowest in winter. This would be due to that the major sources of PM in Taklimakan Desert are not anthropogenic emissions but the dust emissions which are usually largest in spring due to the frequent strong dust storms. Figure 4 further shows an example of the hourly results of PM reanalysis, which presents a year-round time series of site mean hourly PM concentrations over Beijing. It shows that the PM reanalysis well captures the hourly evolution of the PM concentrations. Both the heavy haze episodes during wintertime and the strong dust storms during the springtime can be well represented in the PM reanalysis.

https://doi.org/10.5194/essd-2020-100
Preprint. Discussion started: 2 June 2020

4.1.2 Assessment of PM reanalysis over China

The cross validation (CV) method was used to assess the quality of PM reanalysis in China. Table 2 summarized the site-based CV results for the reanalysis data from 2013 to 2018 at different temporal scales. It is pertinent to mention here that these sites are all validation sites that were not used in the data assimilation. The validation results indicate that by assimilating the surface PM concentrations, the reanalysis shows much better performances in reproducing the magnitude and variability of surface PM concentrations in China. The CV R^2 were up to 0.81 and 0.72 for the hourly concentrations of $PM_{2.5}$ and PM_{10}, significantly higher than the values of 0.26 and 0.17 in the base simulation. The biases were reduced substantially in $PM_{2.5}$ and PM_{10} reanalysis with CV MBE (CV NMB) about -2.6 μg/m^3 (-4.9%) and -6.8 μg/m^3 (-8.7%) at the hourly scale, much smaller than the large biases in the base simulation. The CV RMSE were only about one half of the RMSE values of the base simulation, which were about 17.6 μg/m^3 and 39.3 μg/m^3 for the hourly concentrations of $PM_{2.5}$ and PM_{10}. The reanalysis shows better performance at the daily, monthly and yearly scale with CV RMSE values ranging from 9.0 to 15.1 μg/m^3 for $PM_{2.5}$ concentrations and from 19.1 to 28.8 μg/m^3 for PM_{10} concentrations.

The qualities of $PM_{2.5}$ and PM_{10} reanalysis data in different regions of China were further summarized in Table S1-2. At the hourly scale, there were small negative biases of $PM_{2.5}$ reanalysis in the NCP (-4.8%), NE (-5.8%), SE (-3.8%) and SW (-3.4%) regions. The biases were relatively larger in the NW and Central regions, with CV NMB about -7.3% and -8.2%, respectively. Two reasons might help explain the lager biases in these two regions. Firstly, the observation sites are sparser in the NW and Central regions. As a result, the $PM_{2.5}$ concentrations cannot be well constrained at some sites in cross validation. Secondly, the emissions of $PM_{2.5}$ and its precursors might be too low in these two regions, leading to the underestimations of background errors since we only considered the emission uncertainty in the ensemble simulation. Although this problem has been alleviated by using the inflation technique that compensates the missing errors, the overconfident model results could still to some extent degrade the performance of assimilation, making the analysis less influenced by the observations. The errors of $PM_{2.5}$ reanalysis exhibited apparent spatial differences (Table S1). The CV RMSE were smallest in the SE (14.9 μg/m^3) and SW (16.5 μg/m^3) regions, and increased to around ~25 μg/m^3 in the NCP, NE and Central regions. Consistent with the bias distributions, the largest CV RMSE value was found in the NW region which could up to 52.1 μg/m^3, but is still significant smaller than the RMSE value of base simulation (73.0 μg/m^3). The errors of $PM_{2.5}$ reanalysis were smaller at the daily, monthly and yearly scales, with CV RMSE about 10.6–39.4 μg/m^3 at the daily scale, 7.4–26.9 μg/m^3 at the monthly scale and 6.1–23.5 μg/m^3 at the yearly scale. In term of the hourly PM_{10} reanalysis, the CV results (Table S2) showed that there were small negative biases in the NCP, NE, SE and SW regions, ranging from -9.6% of NE to -5.9 of SE. The biases were larger over the NW and Central regions with CV NBM increasing to about 18.0% and 14.1% respectively. The errors of PM_{10} reanalysis also exhibited spatial heterogeneity. The CV RMSE was smallest in the SE (26.0 μg/m^3) and SW (30.2 μg/m^3) regions, and increased to about 39.8 and 43.7 μg/m^3 in the NE and NCP regions. The largest errors were found in the Central and NW regions with CV RMSE about 105.5 and 57.3 μg/m^3 respectively. The PM_{10} reanalysis shows smaller error

https://doi.org/10.5194/essd-2020-100
Preprint. Discussion started: 2 June 2020


Open Access Earth System Science Data Discussions

at the daily, monthly and yearly scale, with CV RMSE about 18.6–85.5 $\mu g/m^3$ at the daily scale, 13.7–64.0 $\mu g/m^3$ at the monthly scale and 12.3–55.8 $\mu g/m^3$ at the yearly scale.

4.1.3 Trend analysis of PM reanalysis over China

A realistic representation of the observed interannual change is another important aspect of the reanalysis dataset. The performance of the reanalysis data in representing the observed interannual change of $PM_{2.5}$ and PM_{10} concentrations was thus evaluated nationwide and over different regions of China. Figure 5–6 display the time series of the monthly mean $PM_{2.5}$ and PM_{10} concentrations nationwide and in different regions. The observed national $PM_{2.5}$ concentrations showed a profound seasonal circle with the highest concentrations in winter and the smallest in summer. The annual trends of $PM_{2.5}$ and PM_{10} concentrations were also calculated using the Mann-Kendall (M-K) trend test and the Theil-Sen trend estimation method, which were summarized in Table 3. There was significant negative trend observed in $PM_{2.5}$ concentrations nationwide, with calculated annual trend about -5.8 ($p<0.05$) $\mu g \cdot m^{-3} \cdot yr^{-1}$. The NE and NCP regions exhibited the largest negative trends among the six regions, with calculated trend about -7.5 ($p<0.05$) and -7.0 ($p<0.05$) $\mu g \cdot m^{-3} \cdot yr^{-1}$, respectively. In other regions, the negative trends were ranging from -6.3 to -5.2 $\mu g \cdot m^{-3} \cdot yr^{-1}$. The base simulation reproduced the observed seasonal cycle of $PM_{2.5}$ concentrations well in all regions. The magnitude of $PM_{2.5}$ concentrations in year 2013 were also well captured in different regions, suggesting that the emission inventories in 2010 were generally reasonable for the simulations of $PM_{2.5}$ in 2013. However, starting from the year 2014 the base simulation tended to overestimate the observations in the NCP, SE and SW regions, indicating that the emission inventory for 2010 may be too high for the simulations of $PM_{2.5}$ concentrations over these regions after 2014. In contrast, the base simulation significantly underestimated the $PM_{2.5}$ concentrations in the NW region. The model performance of base simulation was relatively better in the NE and Central regions throughout the six years. Although the base simulation captured the negative trends of the observed $PM_{2.5}$ concentrations in China and in different regions, the simulated trends were much weaker than these indicated by the observations. Since we used the same emission inventory in the simulations of air pollutants in different years, the simulated trends in the base simulation were only driven by the variations of meteorology conditions. This suggests that the change of meteorology conditions can only explain a small proportion of the negative trends in $PM_{2.5}$ levels in China, and that the emission reductions would contribute more to the decline of $PM_{2.5}$ concentrations. The cross validation run agrees better with the observations. The observed trends of $PM_{2.5}$ concentrations over China and each subregion were all well captured by the reanalysis in the cross validation run. Similar results could be obtained for the analysis of the trend of PM_{10} concentrations, as shown in Fig. 6. The observed PM_{10} concentrations exhibit significant negative trends too, which were well captured by the PM_{10} reanalysis in cross validation run. The base simulation showed better performance in reproducing the PM_{10} levels in China than the $PM_{2.5}$ concentrations, while there were significant underestimations of PM_{10} concentrations in the NW and Central regions. The calculated negative trends of base simulation were still smaller than these given by the observations. This again highlights the large contributions of the emission reduction to the improvement of the air quality in China over these years.

https://doi.org/10.5194/essd-2020-100
Preprint. Discussion started: 2 June 2020

4.1.4 Independent validations of $PM_{2.5}$ reanalysis

Besides the cross validation, the $PM_{2.5}$ reanalysis was further validated against the independent dataset from the U.S. Department of State Air Quality Monitoring Program over China (http://www.stateair.net/, last access: 17 Apr, 2020) , which contains hourly $PM_{2.5}$ concentrations in Beijing, Chengdu, Guangzhou, Shanghai and Shenyang cities. Table 4 presents the comparisons of the observed $PM_{2.5}$ concentrations with these obtained from the CAQRA and base simulation. The results indicate that the $PM_{2.5}$ reanalysis agrees better with the observed magnitude and variability of $PM_{2.5}$ concentrations in all cities. Both the MBE and RMSE were greatly reduced in CAQRA, which were only ranging from -7.1 to -0.3 $\mu g \cdot m^{-3}$ and from 16.8 to 33.6 $\mu g \cdot m^{-3}$, respectively, in these cities. The correlation coefficient was also greatly improved in CAQRA (R^2 = 0.74–0.86) when compared to the base simulation (R^2 = 0.09–0.38). These results confirm that the CAQRA has a high quality in representing the $PM_{2.5}$ pollution in China during these years.

4.1.5 Comparisons with the satellite-estimated $PM_{2.5}$ concentrations

Previous studies have shown that estimating the ground-based $PM_{2.5}$ concentrations from satellite-derived AOD is an effective way to map the $PM_{2.5}$ concentrations in a good accuracy. To further illustrate the accuracy of our $PM_{2.5}$ reanalysis data, we also compared the accuracy of our $PM_{2.5}$ reanalysis data to that of the satellite-estimated $PM_{2.5}$ concentrations. Table 5 summarized several representative studies that focus on the estimations of ground-based $PM_{2.5}$ concentrations in China at the national level using different kinds of methods. Most of these studies estimated the ground-based $PM_{2.5}$ concentrations at the daily scale since they used the polar-orbiting satellite data (e.g. MODIS) that only provide the daily observations of AOD. Estimation conducted by Liu et al., 2019 was an exception that has an hourly resolution since they used the AOD measurement from the geostationary satellite (Himawari-8). The horizontal resolutions of these studies were mainly around 10km except that of Lin et al., 2018 having the finest horizontal resolution (1km) and that of Zhan et al., 2017 having the coarsest horizontal resolution (0.5°). There are few studies provide the long-term $PM_{2.5}$ data covering the recent years. In comparison, our $PM_{2.5}$ reanalysis data can provide the long-term data over China with fine temporal (1h) and high accuracy. A fine temporal resolution is important for the epidemiological studies, especially for the assessment of acute health effects of air pollution. Furthermore, the accuracy of our reanalysis data (CV R^2 = 0.86, CV RMSE = 15.1 $\mu g \cdot m^{-3}$) was also higher than most of these satellite estimates (CV R^2 = 0.56–0.86, CV RMSE = 15.0–20.2 $\mu g \cdot m^{-3}$).

4.2 Gases

4.2.1 Spatial distributions of the reanalysis of gaseous air pollutants over China

Next, we present the reanalysis fields for the gaseous air pollutants in China, namely SO_2, CO, NO_2 and O_3. Figure 7 presents the spatial distributions of the six-year averaged SO_2 and CO concentrations in China obtained from CAQRA, base simulation and observations. The SO_2 reanalysis well captured the magnitude and spatial distributions of SO_2 concentrations

https://doi.org/10.5194/essd-2020-100
Preprint. Discussion started: 2 June 2020

in China, while the base simulation significantly overestimated the SO_2 concentrations due to the positive biases of SO_2 emissions in the simulation. Consistent with the observations, the SO_2 reanalysis exhibited high spatial heterogeneity with highest values located in the NCP region, especially in Shandong, Shanxi and Hebei provinces. Several hotspots of SO_2 concentrations were also found in the NE region. SO_2 is mainly emitted from the fossil fuel consumption, especially the burning of coal (Lu et al., 2010). Shandong, Shanxi, Inner Mongolia and Hebei provinces were the largest four consumers of coal in China according to the China Energy Statistical Yearbook (NBSC 2017a, b), which well explained the high SO_2 concentrations in these provinces. We also found observable SO_2 concentrations in the Xizang province which were missing in the base simulation. The spatial distribution of the CO reanalysis is similar to that of the SO_2 and agreed well with the observed spatial distributions. In contrast, the base simulation significantly underestimated the CO concentrations, especially in the NCP region. In addition, both the observation and reanalysis show hotspots of CO concentrations in the NW region and Xizang provinces, while these hotspots were largely underestimated or even missing in the base simulation. According to previous studies, such underestimation might be related to the underestimated CO emissions in China (Kong et al., 2020; Tang et al., 2013). For NO_2 (Fig. 8), both the reanalysis and base simulation captured the observed magnitude and spatial distributions of NO_2 concentrations in China. The high NO_2 concentrations were generally located in the NCP region and the major city clusters in China. However, the base simulation generally showed underestimations of NO_2 concentrations in China. The spatial distributions of O_3 concentrations (Fig. 8) show smaller spatial heterogeneity compared to the other gases. The O_3 reanalysis captured the observed magnitude and spatial distributions of O_3 concentrations well in China while the base simulation generally showed underestimations of O_3 concentrations in China. Figure S3–6 further presents the seasonal maps of the reanalysis fields of these gases. All gases exhibited a profound seasonal cycle with maximum values seen in the winter and lowest values in summer except the O_3 which showed an opposite seasonal cycle. The largest values of SO_2, CO and NO_2 concentrations in winter would be due to the increased anthropogenic emissions and also the more stable atmosphere conditions during that time. For O_3, the highest value in summer was closely related to the enhanced photochemistry reactions in summer associated with higher temperature and stronger solar radiance.

4.2.2 Assessment of gases' reanalysis over China

The evaluation results of these gases' reanalysis data were shown in Table 2. It indicates that the reanalysis data has an excellent performance in representing the magnitude and variability of these gaseous air pollutants in China with CV R^2 ranging from 0.51 of SO_2 to 0.76 of O_3, and the CV MBE (CV NMB) about -2.0 $\mu g \cdot m^{-3}$ (-8.5%), -2.3 $\mu g \cdot m^{-3}$ (-6.9%), -0.06 $mg \cdot m^{-3}$ (-6.1%) and -2.3 $\mu g \cdot m^{-3}$ (-4.0%) for the hourly SO_2, NO_2, CO and O_3 reanalysis data, respectively. Compared to the base simulation, the errors were reduced by about one half in the reanalysis with CV RMSE about 24.9 $\mu g \cdot m^{-3}$, 16.4 $\mu g \cdot m^{-3}$, 0.54 $mg \cdot m^{-3}$ and 21.9 $\mu g \cdot m^{-3}$ for the hourly SO_2, NO_2, CO and O_3 reanalysis data, respectively. The reanalysis shows better performance at the daily, monthly and yearly scales. The CV RMSE values of the daily SO_2 and NO_2 reanalysis data were also smaller than the previously datasets of SO_2 and NO_2 concentrations in China developed by Zhan et al., 2018;

https://doi.org/10.5194/essd-2020-100
Preprint. Discussion started: 2 June 2020


Open Access Earth System Science Data Discussions

and Zhang et al., 2019 based on the random-forest-spatiotemporal-kriging model wherein the RMSE values of daily SO_2 and NO_2 concentrations were estimated to be 19.5 and 13.3 $\mu g \cdot m^{-3}$.

In terms of different regions (Table S3–6), the hourly SO_2 reanalysis showed small negative biases (about 2–10%) in all regions except in the Central region where the negative biases were relative larger (17.0%). The smallest CV RMSE values of SO_2 reanalysis were observed in the SE, SW and NW regions (less than 25 $\mu g \cdot m^{-3}$) while in other regions the CV RMSE values were over 30 $\mu g \cdot m^{-3}$. The hourly NO_2 reanalysis showed small negative biases in all regions, which were relatively smaller in the NE, NCP and SE regions (from -5.9 to -3.5%) and become relative larger in the SW, NW and Central regions (from -15.1 to -12.9%). The CV RMSE values for hourly NO_2 reanalysis were around 15 $\mu g \cdot m^{-3}$ in all regions except in the NW (24.3 $\mu g \cdot m^{-3}$) and Central (20.5 $\mu g \cdot m^{-3}$) regions. The hourly CO reanalysis exhibited small negative biases in all regions. The largest biases were still found in the NW region which were about 15.0%, while in other regions the biases were ranging from -11.2% to -2.5%. The CV RMSE values for hourly CO reanalysis were smallest in the south China (about 0.39 and 0.46 $mg \cdot m^{-3}$ in the SE and SW regions) and increased to 0.64 and 0.59 $mg \cdot m^{-3}$ in the NCP and NE regions. The largest CV RMSE was found in the NW regions, which were about 1.13 $mg \cdot m^{-3}$. The biases of hourly O_3 reanalysis were more uniformly distributed in different regions, with CV NMB ranging from -6.1% to 1.4%. Similarly, the CV RMSE values of O_3 reanalysis were around 20 $\mu g \cdot m^{-3}$ in all regions except in the NW region (28.3 $\mu g \cdot m^{-3}$).

4.2.3 Trend analysis of gases' reanalysis over China

Figure 9 shows the time series of the monthly mean SO_2 concentrations in China obtained from cross validation run, base simulation and observations. Also shown are the time series of the monthly mean SO_2 concentrations in different regions. The observed SO_2 concentrations show significant negative trends ($P<0.05$) in China (-6.2 $\mu g \cdot m^{-3} \cdot yr^{-1}$, Table 6) and in all regions (from -2.3 to -9.5 $\mu g \cdot m^{-3} \cdot yr^{-1}$, Table 4) due to the large reductions in SO_2 emissions over China. During the 11-13rd Five-Year Plan (FYP) and the Air Pollution Prevention and Control Plan, Chinese government has taken great efforts to reduce the SO_2 emissions, such as the installations of flue-gas desulfurization (FGD) and selective catalytic reduction system, the construction of large units, decommissioning of small units and replacing coal with cleaner energies (Li et al., 2017; Zheng et al., 2018b). As a result, the SO_2 emissions were substantially decreased in China especially for the industrial and power sectors. The base simulation significantly overestimated the SO_2 concentrations in all regions especially after year 2013. The negative trends of SO_2 concentrations were also largely underestimated by the base simulation. In contrast, the SO_2 reanalysis well captured the magnitude and negative trends of the observed SO_2 concentrations in China and in all regions. The NO_2 observations showed negative trends in China as well (Fig. 10), however the negative trend was not significant except that in the NE region (Table 5). This is consistent with the smaller reductions of NO_x emissions (21%) in China due to the smaller changes in the emissions from transportation sector which accounts for almost one third of the NO_x emissions in China. The pollution controls on the transportation section were exactly offset by the growing emissions related to the vehicle growth (Zheng et al., 2018b). The base simulation generally underestimated the NO_2 concentrations during the wintertime, and the

https://doi.org/10.5194/essd-2020-100
Preprint. Discussion started: 2 June 2020

observed negative trends of NO_2 concentrations were also underestimated in all regions. By assimilating the observed NO_2 concentrations, the reanalysis data agreed better with the observations both for the magnitude and the negative trends. The CO observations showed significant negative trends in all regions except in the NW region (Fig. 11) with calculated negative trends ranging from -0.18 to -0.06 $\mu g \cdot m^{-3} \cdot yr^{-1}$. Such negative trends were also observed by the satellite measurements such as the MOPITT observations (Zheng et al., 2018a), which were mainly due to the reduced anthropogenic emissions in China as suggested by both the bottom-up and top-down methods (Zheng et al., 2019). The base simulation largely underestimated the CO concentrations in all regions. In addition, the negative trends of CO concentrations were also largely underestimated by the base simulation which highlighted the significant contributions of the emission reduction to the decreased CO concentrations in these regions. The CO reanalysis agreed better with the observations and well captured the negative trends of CO concentrations in all regions. The O_3 concentrations exhibited an opposite trend compared to the other air pollutants (Fig. 12), which exhibited significant positive trends in all regions, ranging from 2.3 to 5.4 $\mu g \cdot m^{-3} \cdot yr^{-1}$ and indicating an enhanced photochemical pollution in China. This phenomenon has been observed and investigated by Li et al., 2019 who suggested that the rapid decreases in $PM_{2.5}$ concentrations and the resultant slowing down of aerosol sink of hydroperoxyl (HO_2) radicals was an important factor for the enhanced O_3 concentrations in China. The base simulation generally captured the magnitude of the O_3 concentrations in the SE, SW, NW and Central regions but underestimated the O_3 concentrations in the NCP and NE regions especially during the spring and summer. In addition, the base simulation underestimated the observed positive trend of O_3 concentrations in all regions, which suggests that the meteorological variability only contributed a small portion of the observed O_3 trend in China. Again, the O_3 reanalysis is substantially improved compared to the base simulation and well reproduced the observed trends of O_3 concentrations in each region.

4.2.4 Comparison with the CAMS reanalysis data

In order to further evaluate the accuracy of our reanalysis dataset for the gaseous air pollutants, the CAMS reanalysis (CAMSRA) produced by the ECMWF (Inness et al., 2019) are employed as a reference to compare with our reanalysis dataset. The CAMSRA is the latest global reanalysis dataset of atmospheric compositions, which assimilates the satellite retrievals of O_3, CO, NO_2 and AOD. Three-hourly reanalysis data of SO_2, NO_2, CO and O_3 concentrations in surface model level from 2013 to 2018 were used in this study, which were downloaded from https://atmosphere.copernicus.eu/copernicus-releases-new-global-reanalysis-data-set-atmospheric-composition (last access: 17 Apr, 2020) at an 1 degree by 1 degree resolution. Here we only focus on the comparisons of gaseous pollutants since the CAMSRA does not provide the $PM_{2.5}$ and PM_{10} concentrations.

Figure 13 presents the spatial distributions of the six-year averaged concentrations of these gaseous air pollutants in China obtained from CAMSRA. Compared with these obtained from CAQRA and observations (Fig. 7–8), the CAMSRA largely overestimates the surface concentrations of SO_2 and O_3 in China. In addition, due to the higher spatial resolution (15km) used in CAQRA than that used in CAMSRA (about 50km), our products can provide more detailed spatial patterns of the surface air pollutants in China, which should be more suitable for the air quality studies in the regional scale. Table 7 quantitatively

https://doi.org/10.5194/essd-2020-100
Preprint. Discussion started: 2 June 2020

compares the accuracy of the CAQRA with that of the CAMSRA in estimating the surface concentrations of gaseous air pollutants in China. Compared with CAMSRA (R^2 = 0.00–0.23), the CAQRA shows much better performance in capturing the spatiotemporal variability in the surface concentrations of gaseous air pollutants in China with R^2 ranging from 0.53 to 0.77. The MBE and RMSE values are also smaller in the CAQRA than these in CAMSRA, especially for the SO_2 and O_3 concentrations. This could be attributed to the assimilation of surface observations in CAQRA, while CAMSRA only assimilate the satellite retrievals. These suggest that the CAQRA can provide surface air quality datasets in China with higher quality than the CAMSRA, which is especially valuable for future relevant studies with high demands in spatiotemporal resolution and accuracy.

5 Conclusions

A high-resolution Chinese Air Quality Reanalysis (CAQRA) Dataset has been produced in this study by assimilating the surface observations of $PM_{2.5}$, PM_{10}, SO_2, NO_2, CO and O_3 concentrations from CNEMC. It provides the time-consistent concentration fields of $PM_{2.5}$, PM_{10}, SO_2, NO_2, CO and O_3 in China from 2013 to 2018 (will be extended in the future by adding 1 year each year) at a high spatial (15km) and temporal (1 hour) resolution. The CAQRA was produced by the ChemDAS which used the NAQPMS model as the forecast model, and the LETKF to assimilate the observations in a post processing mode. The background error covariance was calculated from the ensemble simulation which considered the emission uncertainties of major air pollutants. An inflation technique was also used to dynamically inflate the background error to prevent the underestimation of true background error covariance.

A five-fold cross validation method was used to validate the reanalysis dataset and provides us the first indication of the quality of CAQRA. The validation results suggest that the CAQRA has excellent performance in representing the spatiotemporal variability of surface air pollutants in China with CV R^2 ranging from 0.52 of hourly SO_2 concentrations to 0.81 of hourly $PM_{2.5}$ concentrations. The CV MBE of reanalysis data were -2.6 $\mu g \cdot m^{-3}$, -6.8 $\mu g \cdot m^{-3}$, -2.0 $\mu g \cdot m^{-3}$, -2.3 $\mu g \cdot m^{-3}$, -0.06 $mg \cdot m^{-3}$ and -2.3 $\mu g \cdot m^{-3}$ for the hourly concentrations of $PM_{2.5}$, PM_{10}, SO_2, NO_2, CO and O_3 respectively. The CV RMSE values of the reanalysis data for these air pollutants were estimated to be about 21.3$\mu g \cdot m^{-3}$, 39.3$\mu g \cdot m^{-3}$, 24.9$\mu g \cdot m^{-3}$, 16.4, $\mu g \cdot m^{-3}$, 0.54$mg \cdot m^{-3}$ and 21.9 $\mu g \cdot m^{-3}$, respectively. Over the different regions of China, the NW and Central regions have relative larger biases and errors which would be mainly due to the relatively sparse observations and also the underestimations of background errors. The Chinese air quality has changed substantially over the last six years. the observations show significant decreasing trends for all air pollutants except the O_3 which shows increasing trend over the last six years. The reanalysis data shows excellent performance in representing the trends of all air pollutants in China, suggesting the suitability of the reanalysis data in the trend analysis of air pollutants in China.

Besides the cross validation, the $PM_{2.5}$ reanalysis data has also been evaluated against the independent observations from the U.S. Department of State Air Quality Monitoring Program over China. The results suggest that the reanalysis can well reproduced the magnitude and variability of the observed $PM_{2.5}$ concentrations in all cities with the MBE and RMSE only

https://doi.org/10.5194/essd-2020-100
Preprint. Discussion started: 2 June 2020


Open Access Earth System Science Data Discussions

ranging from -7.1 to -0.3 $\mu g \cdot m^{-3}$ and from 16.8 to 33.6 $\mu g \cdot m^{-3}$, respectively. The reanalysis of gaseous air pollutants was also compared with the latest global reanalysis data CAMSRA from the ECMWF. The CAMSRA is of great values in providing the three-dimensional distributions of multiple chemical species in global. As a regional dataset, our products have higher spatial resolution than the CAMSRA, which could be more suitable for the air quality studies in the regional scale. Although our products only provide the surface concentrations of six conventional air pollutants in China, the accuracy of CAQRA was estimated to be higher than that of the CMSRA due to the assimilations of surface observations. Thus, our products have its own values in the regional air quality studies with high demands in spatiotemporal resolution and accuracy We also compared our $PM_{2.5}$ reanalysis data to the previous satellite estimates of surface $PM_{2.5}$ concentrations, which shows that the $PM_{2.5}$ reanalysis data is more accurate than most of satellite estimates and has finer temporal resolution.

As the first version of Chinese air quality reanalysis data, there were still limitations in the CAQRA that the potential users should be aware of. The current CAQRA only contains the surface concentrations of the air pollutants in China which cannot provide the information on the vertical structure of the air pollutants. Besides, the observation sites used in the assimilation are mainly urban or suburban sites that cannot provide enough information on the air pollution over the rural areas, which may influence the quality of CAQRA over the rural areas. To further improve the accuracy of our air quality reanalysis dataset, in future, an online run of EnKF could be conducted to simultaneously correct the emissions and concentrations. More kinds of observations, such as the observation data of $PM_{2.5}$ compositions, could also been assimilated to provide the fields of $PM_{2.5}$ composition in China, which would support both the epidemiological studies and climate research.

Data availability

The whole CAQRA reanalysis dataset can be freely downloaded at: https://doi.org/10.11922/sciencedb.00053 (Tang et al., 2020a), and the teaser product, which contains the monthly and annual mean of the CAQRA, is available at https://doi.org/10.11922/sciencedb.00092 (Tang et al., 2020b).

Author contributions

X.T., J.Z., and Z.W. conceived and designed the project; H.W., L.K., X.T., L.W. established the data assimilation system; Q.W. and L.K. performed the meteorology simulation; X.T., L.K., H.C., H.W., H.Z., G.J. and M.L. performed the ensemble simulation of NAQPMS; J.L., L.Z., W.W., B.L., Q.W., D.C. and T.S. provided the air quality monitoring data. W.H. performed the quality control of the observation data and F.L. estimated the representativeness error of observations; L.K. conducted the calculation of CAQRA, drew figures and wrote the paper with the comments from G.C.

https://doi.org/10.5194/essd-2020-100
Preprint. Discussion started: 2 June 2020

Open Access Earth System Science Data Discussions

Competing interests

The authors declare that they have no conflict of interest.

Acknowledgements

This study was funded by the National Natural Science Foundation (Grant Nos. 91644216, 41575128, 41875164), the CAS Strategic Priority Research Program (Grant No. XDA19040201), the CAS Information Technology Program (Grant No. XXH13506-302)

Tables

Table 1 Uncertainties in the emissions of different species

Species	SO_2[a]	NO_x[a]	CO[a]	NMVOC[a]	NH_3[b]	PM_{10}[a]	$PM_{2.5}$[a]	BC[a]	OC[a]
Emission Uncertainty(%)	±12	±31	±70	±68	±53	±132	±130	±208	±258

[a] emission uncertainty obtained from Zhang et al., 2009

[b] emission uncertainty obtained from Streets et al., 2003

https://doi.org/10.5194/essd-2020-100
Preprint. Discussion started: 2 June 2020

Open Access Earth System Science Data Discussions

Table 2: Site-based cross validation results for the reanalysis data (outside bracket) and base simulation (in bracket) from 2013 to 2018 at different temporal scales.

	$PM_{2.5}$ ($\mu g/m^3$)				PM_{10} ($\mu g/m^3$)			
	R^2	MBE	NMB(%)	RMSE	R^2	MBE	NMB (%)	RMSE
Hourly	0.81 (0.26)	-2.6 (17.6)	-4.9 (34.7)	21.3 (54.1)	0.72 (0.17)	-6.8 (-7.6)	-7.8 (-8.7)	39.3 (75.7)
Daily	0.86 (0.32)	-2.5 (17.4)	-4.9 (34.3)	15.1 (46.4)	0.81 (0.22)	-6.7 (-7.0)	-7.7 (-8.1)	28.8 (64.1)
Monthly	0.88 (0.40)	-2.5 (17.4)	-5.0 (34.1)	10.3 (33.6)	0.83 (0.28)	-6.7 (-7.3)	-7.7 (-8.4)	21.1 (44.4)
Yearly	0.86 (0.37)	-3.0 (15.2)	-5.6 (28.7)	9.0 (28.9)	0.79 (0.27)	-7.5 (-10.2)	-8.3 (-11.3)	19.1 (38.2)
	SO_2 ($\mu g/m^3$)				NO_2 ($\mu g/m^3$)			
	R^2	MBE	NMB(%)	RMSE	R^2	MBE	NMB (%)	RMSE
Hourly	0.52 (0.03)	-2.0 (25.5)	-8.5 (106.6)	24.9 (67.2)	0.61 (0.22)	-2.3 (-5.0)	-6.9(-14.8)	16.4 (24.9)
Daily	0.67 (0.04)	-2.0 (25.6)	-8.5 (106.9)	17.5 (59.3)	0.67 (0.27)	-2.3 (-5.0)	-6.8(-14.8)	12.3 (19.9)
Monthly	0.74 (0.04)	-2.1 (25.4)	-8.6 (105.7)	13.2 (52.0)	0.67 (0.34)	-2.3 (-5.0)	-6.8 (-14.8)	10.0 (15.9)
Yearly	0.71 (0.04)	-2.6 (23.1)	-9.9 (87.2)	12.0 (47.5)	0.62 (0.42)	-2.5 (-5.9)	-7.3 (-17.3)	9.1 (13.6)
	CO (mg/m^3)				O_3 ($\mu g/m^3$)			
	R^2	MBE	NMB(%)	RMSE	R^2	MBE	NMB (%)	RMSE
Hourly	0.55 (0.17)	-0.06 (-0.47)	-6.1 (-44.7)	0.54 (0.87)	0.76 (0.35)	-2.3 (-10.5)	-4.0 (-17.8)	21.9 (38.3)
Daily	0.61 (0.20)	-0.06 (-0.47)	-5.8 (-44.6)	0.44 (0.77)	0.74 (0.25)	-2.3 (-10.4)	-3.9 (-17.8)	16.6 (31.3)
Monthly	0.62 (0.21)	-0.06 (-0.47)	-6.0 (-44.7)	0.36 (0.69)	0.74 (0.28)	-2.3 (-10.4)	-3.9 (-17.8)	13.1 (25.3)
Yearly	0.52 (0.09)	-0.08 (-0.51)	-6.9 (-46.7)	0.37 (0.72)	0.53 (0.03)	-2.2 (-9.8)	-3.8 (-17.2)	10.4 (21.2)

https://doi.org/10.5194/essd-2020-100
Preprint. Discussion started: 2 June 2020

Open Access Earth System Science Data Discussions

Table 3: Calculated annual trends of the $PM_{2.5}$ and PM_{10} concentrations in China

	$PM_{2.5}$ (μg/m^3)			PM_{10} (μg/m^3)		
	Obs	Cross validation	Base simulation	Obs	Cross validation	Base simulation
China	**-5.8 (-13.4, -3.5)**[a]	**-5.0 (-12.6, -3.1)**	**-2.0 (-3.6, -0.7)**	**-7.2 (-18.4, -3.2)**	**-6.0 (-17.0, -2.9)**	**-2.5 (-3.6, -0.7)**
NCP	**-7.0 (-15.7, -5.5)**	**-6.6 (-14.5, -4.8)**	**-3.5 (-4.7, -1.9)**	**-8.3 (-20.4, -5.1)**	**-7.6 (-19.2, -4.4)**	**-4.2 (-4.7, -1.9)**
NE	**-7.5 (-11.0, -3.9)**	**-6.7 (-10.0, -3.5)**	**-3.2 (-5.8, -1.2)**	**-11.2 (-17.4, -4.7)**	**-10.4 (-16.4, -4.7)**	**-3.7 (-5.8, -1.2)**
SE	**-5.2 (-11.3, -2.8)**	**-4.9 (-10.6, -2.7)**	-0.9 (-3.1, 1.3)	**-6.0 (-14.9, -2.4)**	**-5.8 (-13.2, -1.9)**	-1.6 (-3.1, 1.3)
SW	**-6.3 (-12.8, -2.6)**	**-4.9 (-12.2, -2.4)**	-1.4 (-7.5, 0.4)	**-7.9 (-19.9, -2.2)**	**-5.5 (-17.5, -2.1)**	**-1.3 (-7.5, 0.4)**
NW	-5.7 (-11.6, 2.1)[b]	-3.3 (-10.7, 1.8)	-1.3 (-4.9, 2.9)	-0.5 (-14.4, 1.6)	-2.2 (-8.5, 3.4)	-2.3 (-4.9, 2.9)
Central	**-5.8 (-19.8, -0.8)**	-3.6 (-17.7, 0.2)	-0.6 (-5.9, 0.9)	-8.9 (-28.5, 0.2)	-6.8 (-26.9, 0.5)	-2.0 (-5.9, 0.9)

[a] the bold font denotes that the calculated trend is significant at the 0.05 significance level and the values in brackets denote the 95% confidence interval

Table 4: Independent validation results of the CAQRA (outside bracket) and the base simulation (in bracket) against the observation data from the U.S. Department of State Air Quality Monitoring Program over China

	R^2	MBE (μg/m^3)	NMB(%)	RMSE (μg/m^3)
Beijing	0.86 (0.37)[a]	-0.3 (11.4)	-0.3 (13.2)	33.6 (75.6)
Shanghai	0.86 (0.34)	5.5 (39.6)	10.9 (78.3)	17.1 (64.8)
Chengdu	0.85 (0.19)	-7.1 (59.3)	-8.9 (74.7)	23.1 (91.5)
Guangzhou	0.74 (0.09)	-3.3 (11.1)	-7.5 (25.1)	16.8 (38.8)
Shenyang	0.85 (0.29)	-2.2 (16.8)	-3.2 (24.3)	24.8 (59.1)

https://doi.org/10.5194/essd-2020-100
Preprint. Discussion started: 2 June 2020

Open Access Earth System Science Data Discussions

Table 5 Comparisons of the accuracy of our $PM_{2.5}$ reanalysis data with that of the satellite estimates

Reference	spatial resolution	temporal resolution	temporal coverage	CV-R^2	CV-RMSE	Method
(Ma et al., 2016)	0.1° ×0.1°	daily	2004–2013	0.79	27.4	LME + GAM
(Xue et al., 2019)	0.1° ×0.1°	daily	2000–2016	0.56	30.2	CTM + HD-expansion + GAM
(Xue et al., 2017)	0.1° ×0.1°	daily	2014	0.72	23.0	CTM + LME + Spatiotemporal Kriging
(Chen et al., 2018)	0.1° ×0.1°	daily	2005–2016	0.83	18.1	RF
(Lin et al., 2018)	1km× 1km	daily	2001 – 2015	0.78[a]	19.3[a]	semi-empirical
(Chen et al., 2019)	3km×3km	daily	2014 – 2015	0.86	15.0	XGBoost + NELRM
(Yao et al., 2019)	6km×6km	daily	2014	0.60	21.8	TEFR + GWR
(You et al., 2016)	0.1° ×0.1°	daily	2014	0.79	18.6	GWR
(Zhan et al., 2017)	0.5° ×0.5°	daily	2014	0.76	23.0	GW-GBM
(Li et al., 2017b)	0.1° ×0.1°	daily	2015	0.82	16.4	Geoi-DBN
(Liu et al., 2019)	0.125° ×0.125°	hourly	2016	0.86	17.3	RF
This study	15km× 15km	hourly	2013–2018	0.81	21.3	EnKF
		daily	2013–2018	0.86	15.1	EnKF

[a] The accuracy of the $PM_{2.5}$ estimates by Lin et al., 2018 was assessed at the monthly scale

LME: Linear Mixed Effect model

GWR: Geographically Weighted Regression model

GAM: Generalized Additive model

HD-expansion: High dimensional expansion

RF: Random Forest

XGBoost: The Extreme Gradient Boosting

NELRM: Non-linear Exposure-lag-response model

TEFR: Time Fixed Effects Regression model

GW-GBM: Geographically-Weighted Gradient Boosting Machine

https://doi.org/10.5194/essd-2020-100
Preprint. Discussion started: 2 June 2020

Table 6: Calculated annual trends of the SO_2, NO_2, CO and O_3 concentrations in China

	SO_2 (μg/m^3)			NO_2 (μg/m^3)		
	Obs	Cross validation	Base simulation	Obs	Cross validation	Base simulation
China	**-6.2 (-12.0, -3.9)** [a]	**-4.9 (-10.3, -3.0)**	**-1.7 (-6.2, -0.8)**	-2.6 (-5.9, 0.1)	-2.1 (-5.9, 0.1)	**-0.9 (-3.0, -0.3)**
NCP	**-9.5 (-16.5, -7.2)**	**-8.1 (-14.5, -5.9)**	**-1.7 (-4.1, -1.4)**	-2.0 (-5.9, 0.0)	-2.1 (-5.6, 0.1)	**-0.6 (-1.6, -0.3)**
NE	**-6.8 (-14.6, -4.9)**	**-5.9 (-12.1, -4.1)**	**-1.8 (-7.6, -0.6)**	**-3.0 (-4.9, -1.1)**	**-3.3 (-5.4, -1.2)**	**-1.3 (-3.8, -0.3)**
SE	**-4.4 (-6.7, -2.5)**	**-3.7 (-5.6, -2.0)**	**-1.0 (-2.9, -0.1)**	-2.4 (-5.3, 0.1)	-2.5 (-5.1, 0.1)	**-1.0 (-1.8, -0.3)**
SW	**-4.2 (-8.8, -1.9)**	**-2.8 (-7.6, -1.3)**	**-3.4 (-15.6, -1.9)**	-1.8 (-6.2, 0.3)	-1.6 (-6.5, 0.2)	**-0.7 (-3.9, -0.2)**
NW	**-2.3 (-11.1, 0.6)**	**-4.2 (-7.7, -1.1)**	-1.9 (-13.7, 1.0)	-3.4 (-8.4, 2.3)	-1.7 (-9.5, 1.3)	-1.0 (-6.5, 0.3)
Central	**-7.9 (-17.5, -3.3)**	**-5.5 (-15.7, -2.3)**	-0.6 (-10.2, 0.0)	-2.0 (-6.6, 1.9)	-1.0 (-8.0, 2.2)	-0.5 (-3.8, 0.1)
	CO (mg/m^3)			O_3 (μg/m^3)		
	Obs	Cross validation	Base simulation	Obs	Cross validation	Base simulation
China	**-0.12 (-0.17, -0.06)**	**-0.12 (-0.18, -0.07)**	**-0.02 (-0.05 -0.01)**	**3.5 (2.1, 5.0)**	**3.8 (2.1, 5.0)**	**2.0 (0.1, 5.9)**
NCP	**-0.18 (-0.25, -0.11)**	**-0.17 (-0.24, -0.11)**	**-0.03 (-0.05, -0.02)**	**5.3 (2.5, 8.7)**	**5.5 (2.4, 8.8)**	1.4 (-0.5, 5.0)
NE	**-0.13 (-0.21, -0.05)**	**-0.13 (-0.20, -0.06)**	**-0.03 (-0.07, -0.01)**	**4.8 (1.5, 10.0)**	**4.6 (1.4, 9.5)**	2.8 (-0.4, 8.0)
SE	**-0.06 (-0.09, -0.04)**	**-0.06 (-0.08, -0.04)**	**-0.01 (-0.02, -0.01)**	**2.3 (0.3, 3.4)**	**2.6 (0.8, 3.5)**	**1.7 (0.3, 3.0)**
SW	**-0.11 (-0.19, -0.04)**	**-0.09 (-0.21, -0.04)**	**-0.02 (-0.06, -0.01)**	**3.2 (1.2, 5.0)**	**3.5 (1.8, 5.4)**	2.7 (-0.9, 7.1)
NW	-0.14 (-0.46, 0.04)	-0.14 (-0.30, 0.04)	-0.03 (-0.06, 0.00)	**5.4 (1.6, 9.8)**	**4.0 (1.4, 10.1)**	2.6 (-0.2, 8.8)
Central	**-0.16 (-0.27, -0.09)**	**-0.17 (-0.25, -0.10)**	-0.01 (-0.06, 0.00)	**5.3 (2.3, 9.2)**	**4.5 (1.4, 7.8)**	2.2 (-0.3, 7.7)

[a] the bold font denotes that the calculated trend is significant at the 0.05 significance level and the values in brackets denote the 95% confidence interval

https://doi.org/10.5194/essd-2020-100
Preprint. Discussion started: 2 June 2020

Table 7: Comparisons of the data accuracy of CAQRA and CAMSRA over China

	CAQRA				CAMSRA			
	SO_2 ($\mu g/m^3$)	NO_2 ($\mu g/m^3$)	CO (mg/m^3)	O_3 ($\mu g/m^3$)	SO_2 ($\mu g/m^3$)	NO_2 ($\mu g/m^3$)	CO (mg/m^3)	O_3 ($\mu g/m^3$)
R^2	0.53	0.61	0.55	0.77	0.04	0.23	0.13	0.00
MBE	-2.0	-2.3	-0.1	-2.3	19.4	1.7	-0.2	30.6
NMB (%)	-8.5	-6.9	-6.1	-4.0	81.2	5.2	-17.5	52.1
RMSE	24.8	16.4	0.5	21.9	54.5	27.3	0.9	55.2

https://doi.org/10.5194/essd-2020-100
Preprint. Discussion started: 2 June 2020

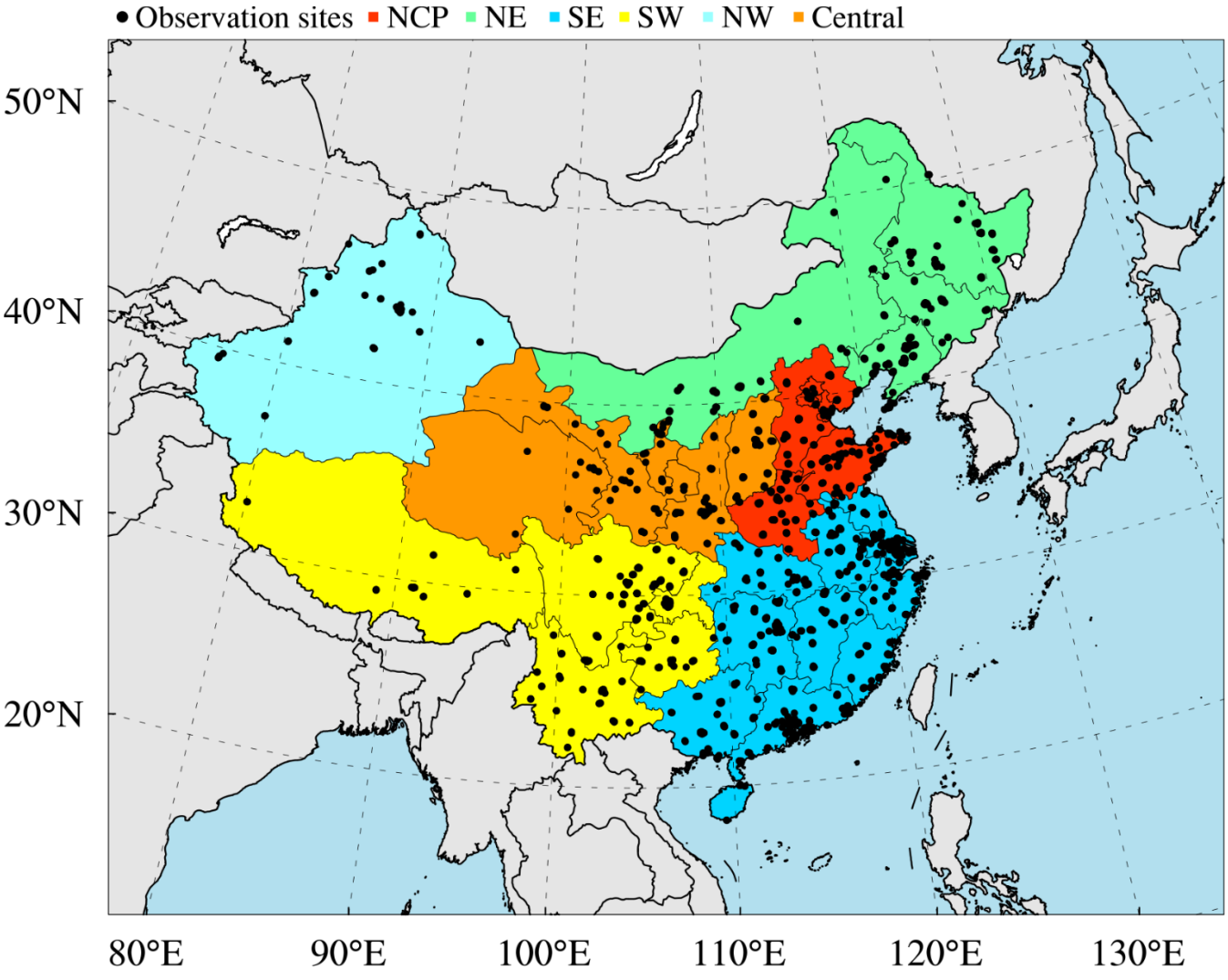

Figures

Figure 1: Modeling domain of the ensemble simulation overlay the distributions of observation sites from CNEMC. Different colours denote the different regions in China, namely North China Plain (NCP), Northeast China (NE), Southwest China (SW), Southeast China (SE), Northwest China (NW) and Central.

https://doi.org/10.5194/essd-2020-100
Preprint. Discussion started: 2 June 2020

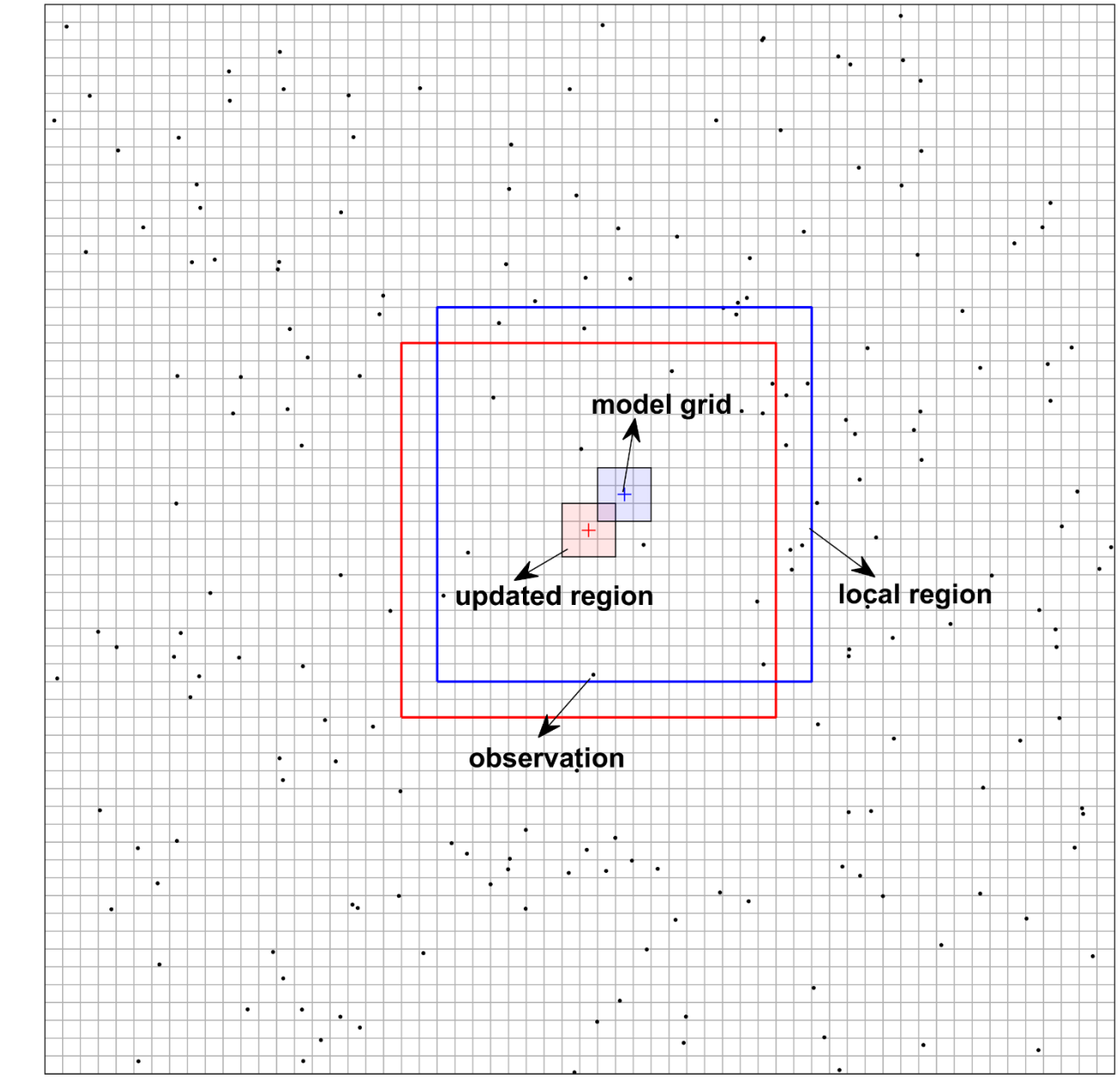

Figure 2: Illustrations of the local analysis scheme used in the assimilation. The plus signs and dots respectively denote the centre of model grids and the location of observation sites. The larger rectangular region denotes the local region and the shaded region denotes the updated region.

https://doi.org/10.5194/essd-2020-100
Preprint. Discussion started: 2 June 2020

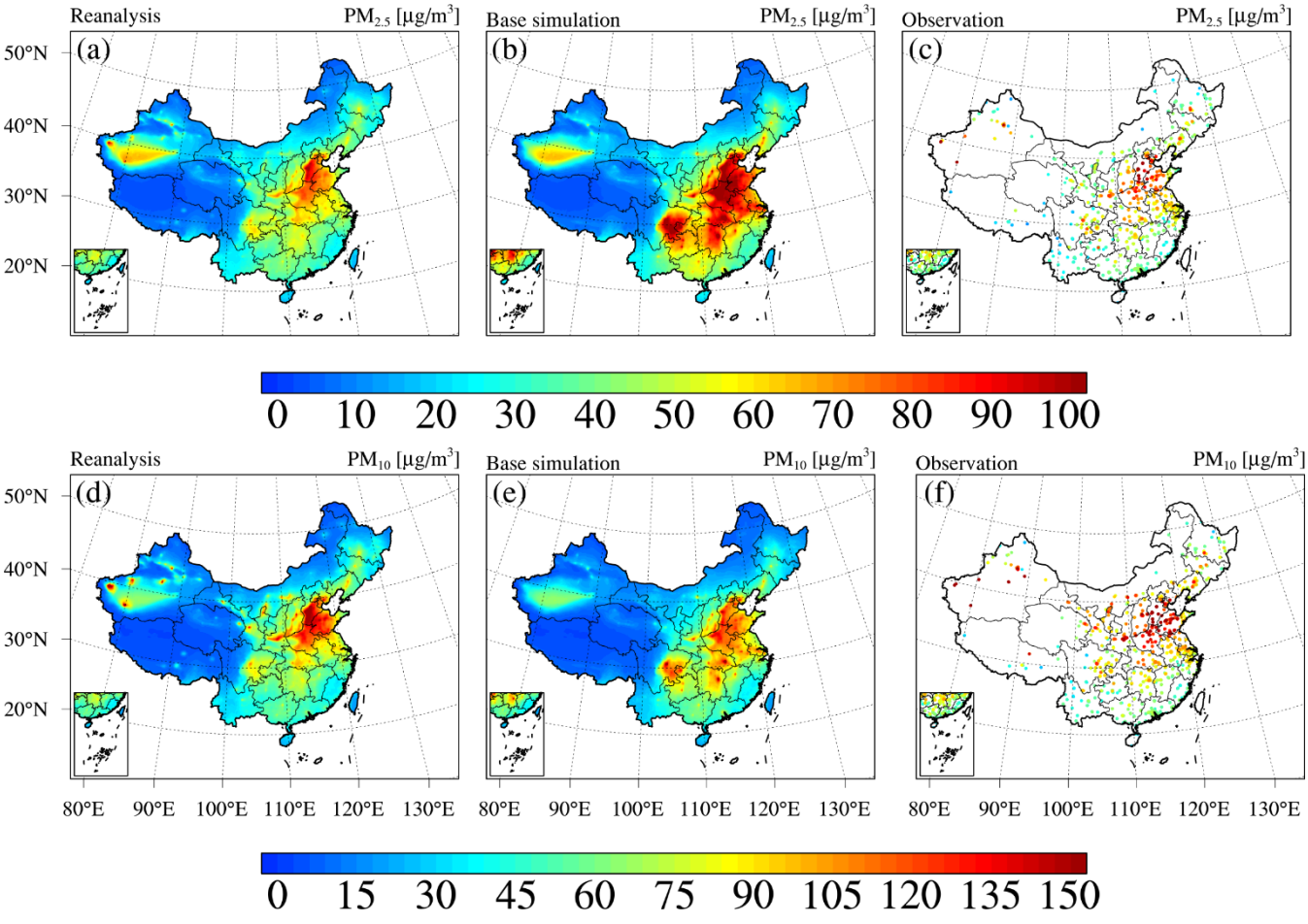

Figure 3: Spatial distributions of the (a–c) $PM_{2.5}$ and (d–f) PM_{10} concentrations in China from (a, d) CAQRA, (b, e) base simulation and (c, f) observations averaged from 2013 to 2018.

5

https://doi.org/10.5194/essd-2020-100
Preprint. Discussion started: 2 June 2020

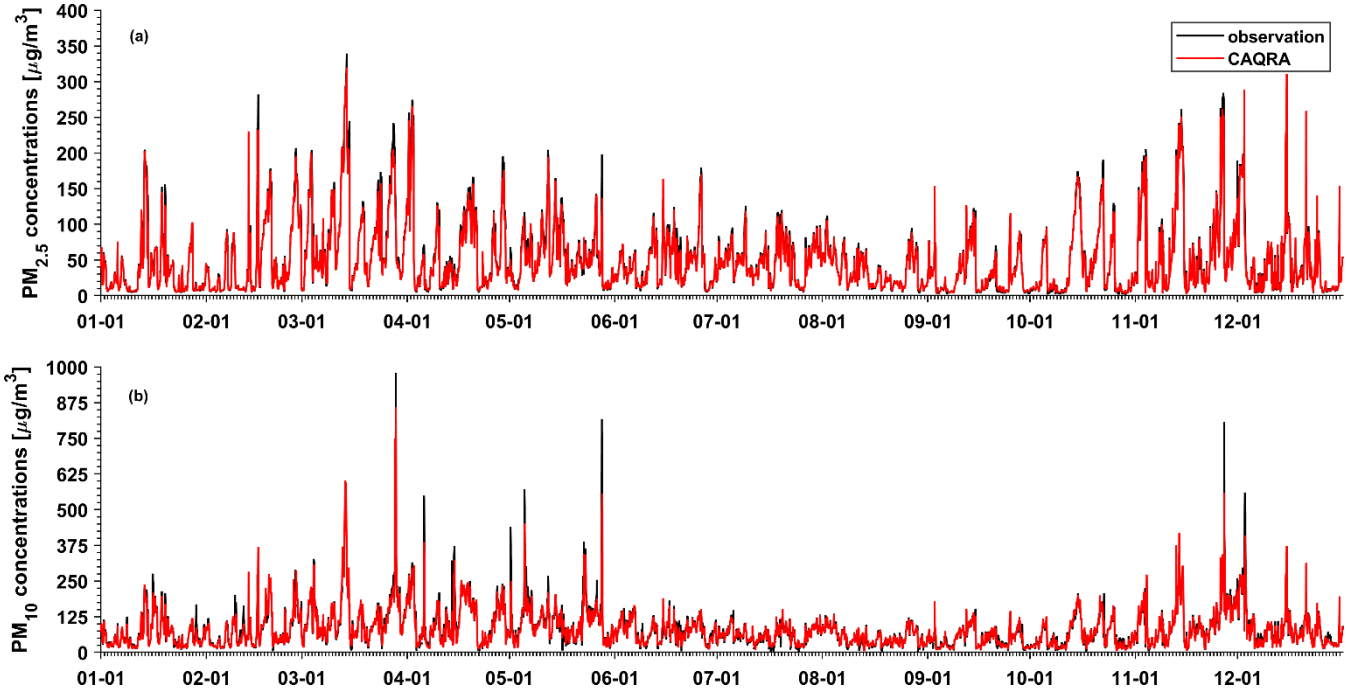

Figure 4: Time series of site mean hourly (a) $PM_{2.5}$ and (b) PM_{10} concentrations in Beijing obtained from observations and CAQRA.

https://doi.org/10.5194/essd-2020-100
Preprint. Discussion started: 2 June 2020

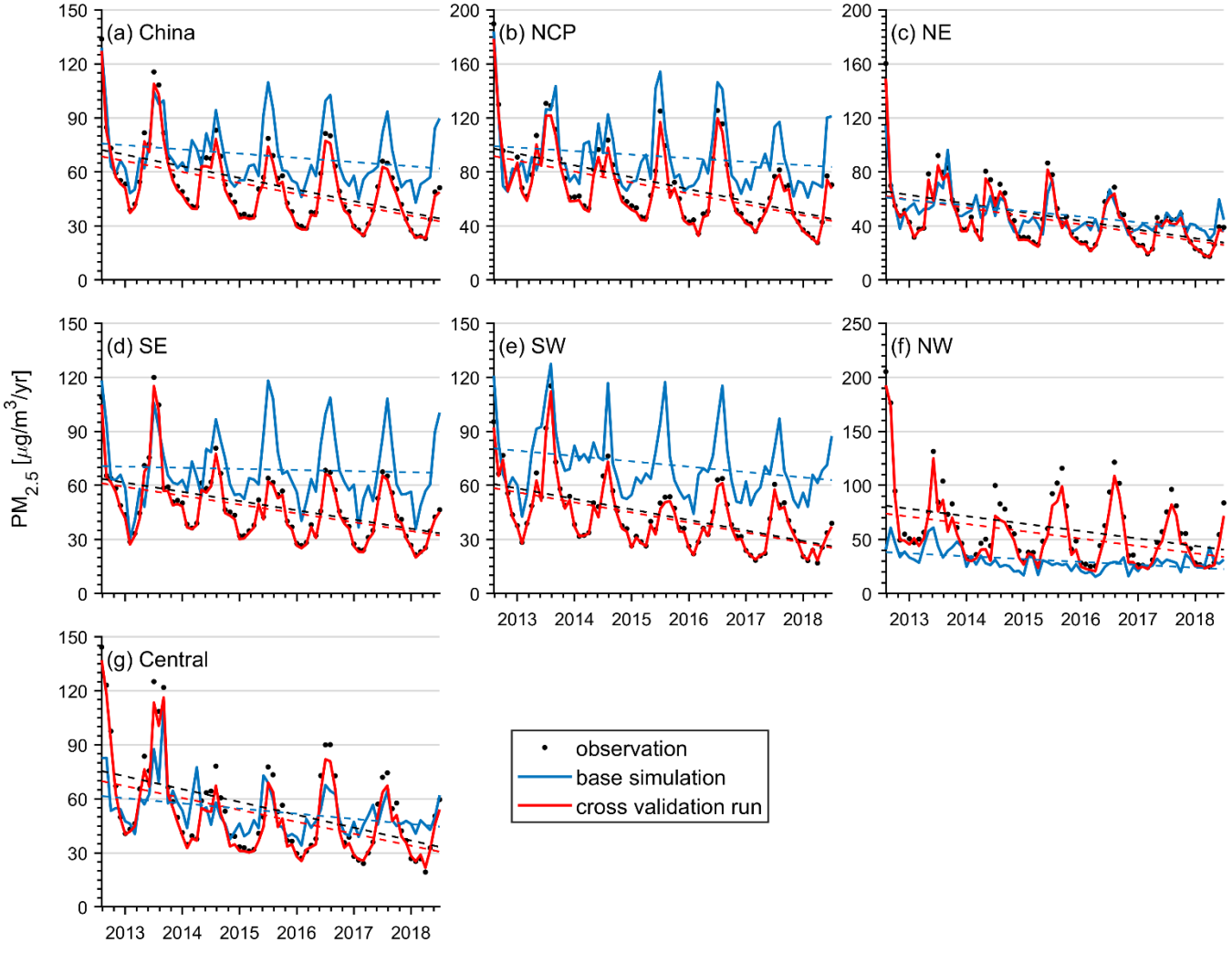

Figure 5: Time series of monthly mean $PM_{2.5}$ concentrations in (a) China, (b) NCP, (c) NE, (d) SE, (e) SW, (f) NW and (f) Central regions obtained from cross validation run (red line), base simulation (blue line) and observations (black dots).

https://doi.org/10.5194/essd-2020-100
Preprint. Discussion started: 2 June 2020

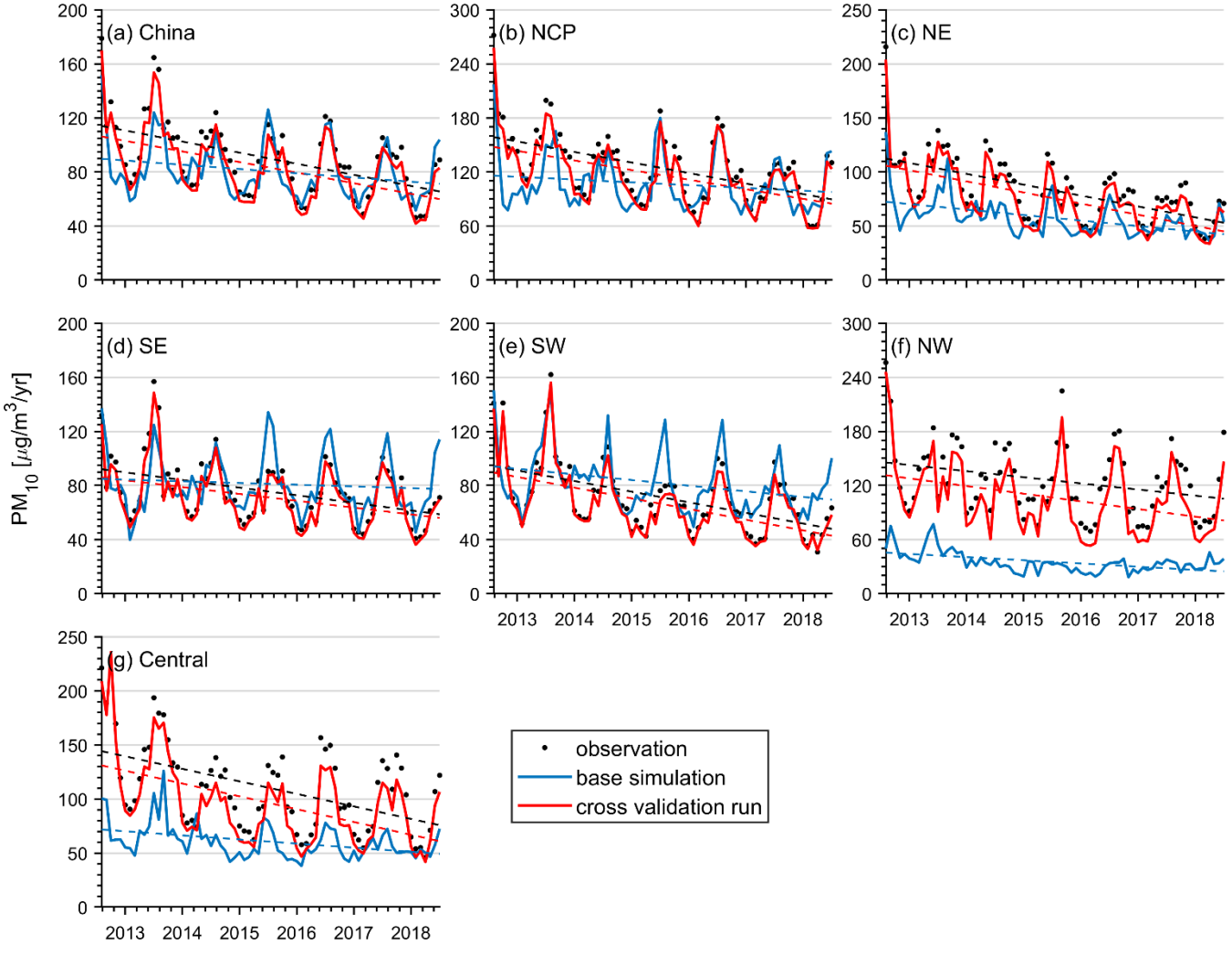

Figure 6: Same as Fig. 5 but for PM_{10} concentrations.

https://doi.org/10.5194/essd-2020-100
Preprint. Discussion started: 2 June 2020

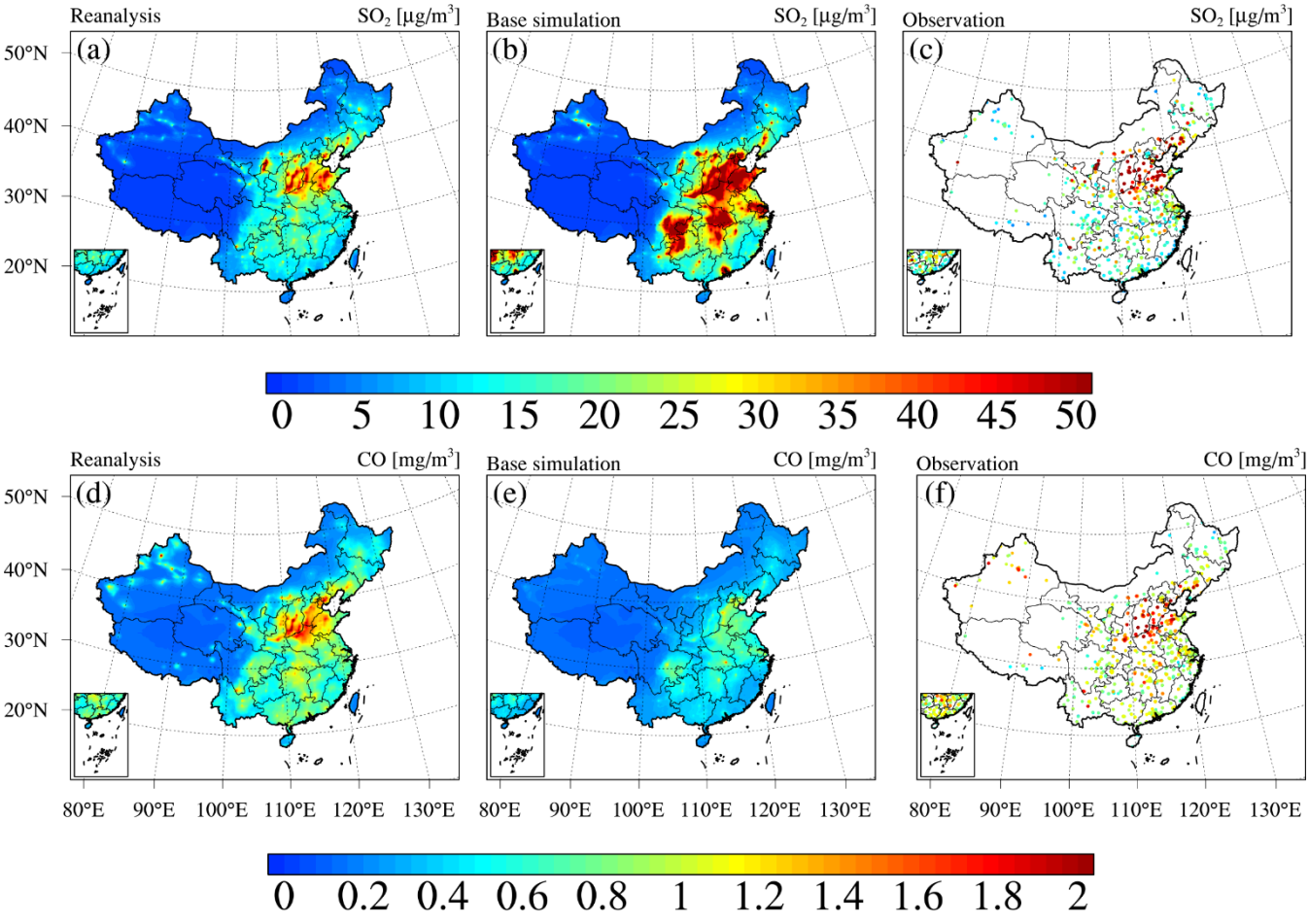

Figure 7: Same as Fig. 3 but for SO_2 and CO concentrations.

https://doi.org/10.5194/essd-2020-100
Preprint. Discussion started: 2 June 2020

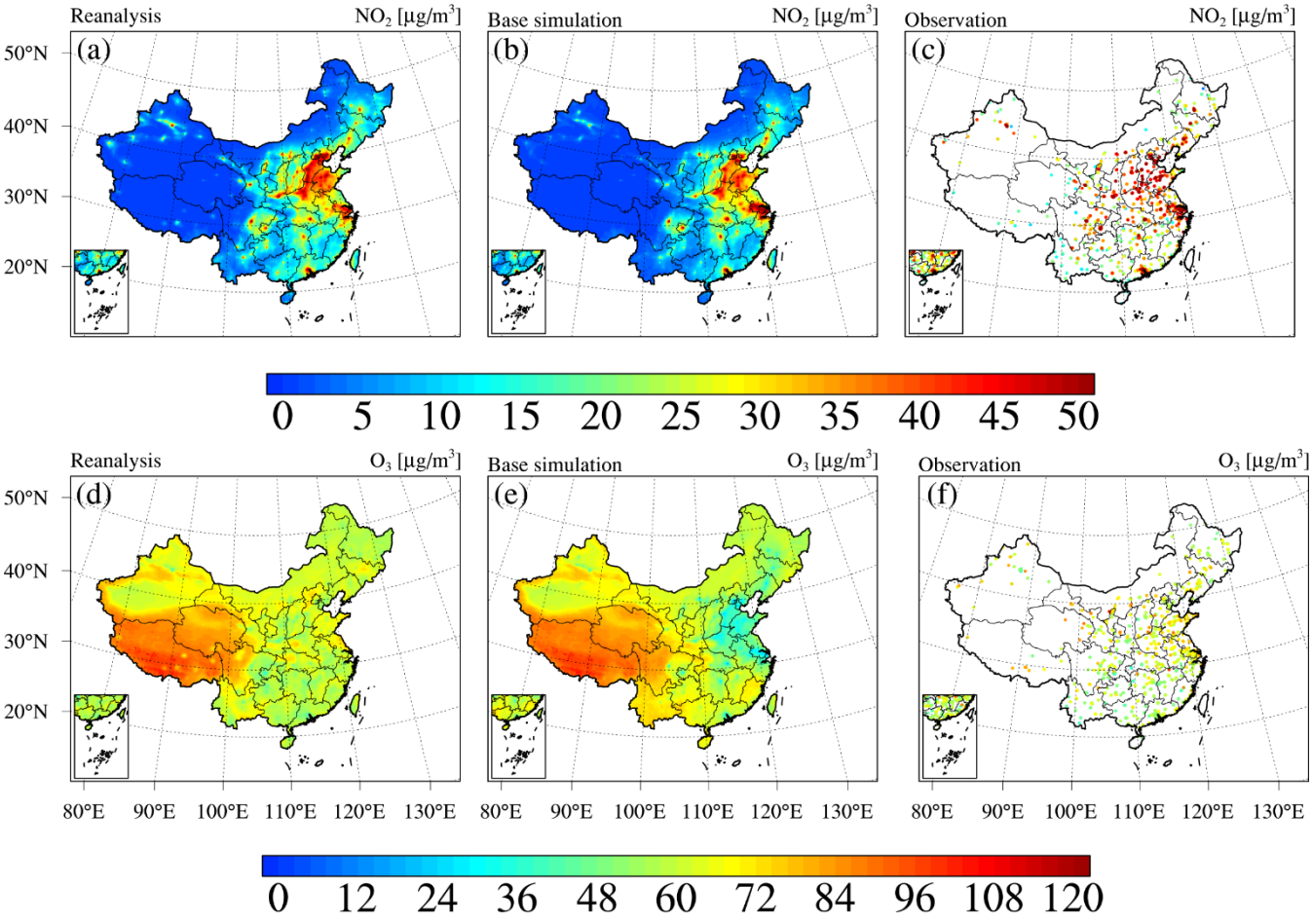

Figure 8: Same as Fig. 3 but for NO_2 and O_3.

https://doi.org/10.5194/essd-2020-100
Preprint. Discussion started: 2 June 2020

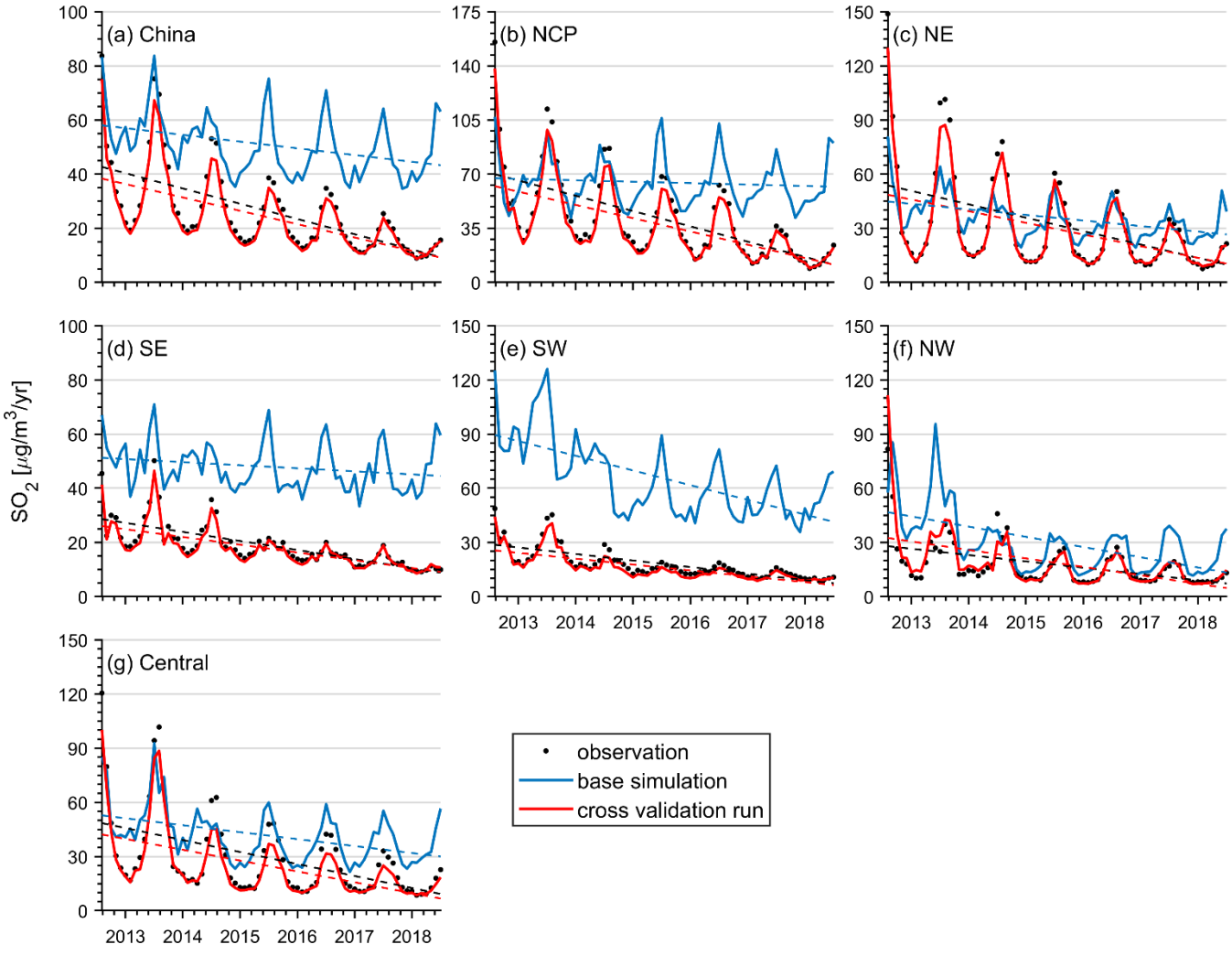

Figure 9: Same as Fig. 5 but for SO_2 concentrations.

https://doi.org/10.5194/essd-2020-100
Preprint. Discussion started: 2 June 2020

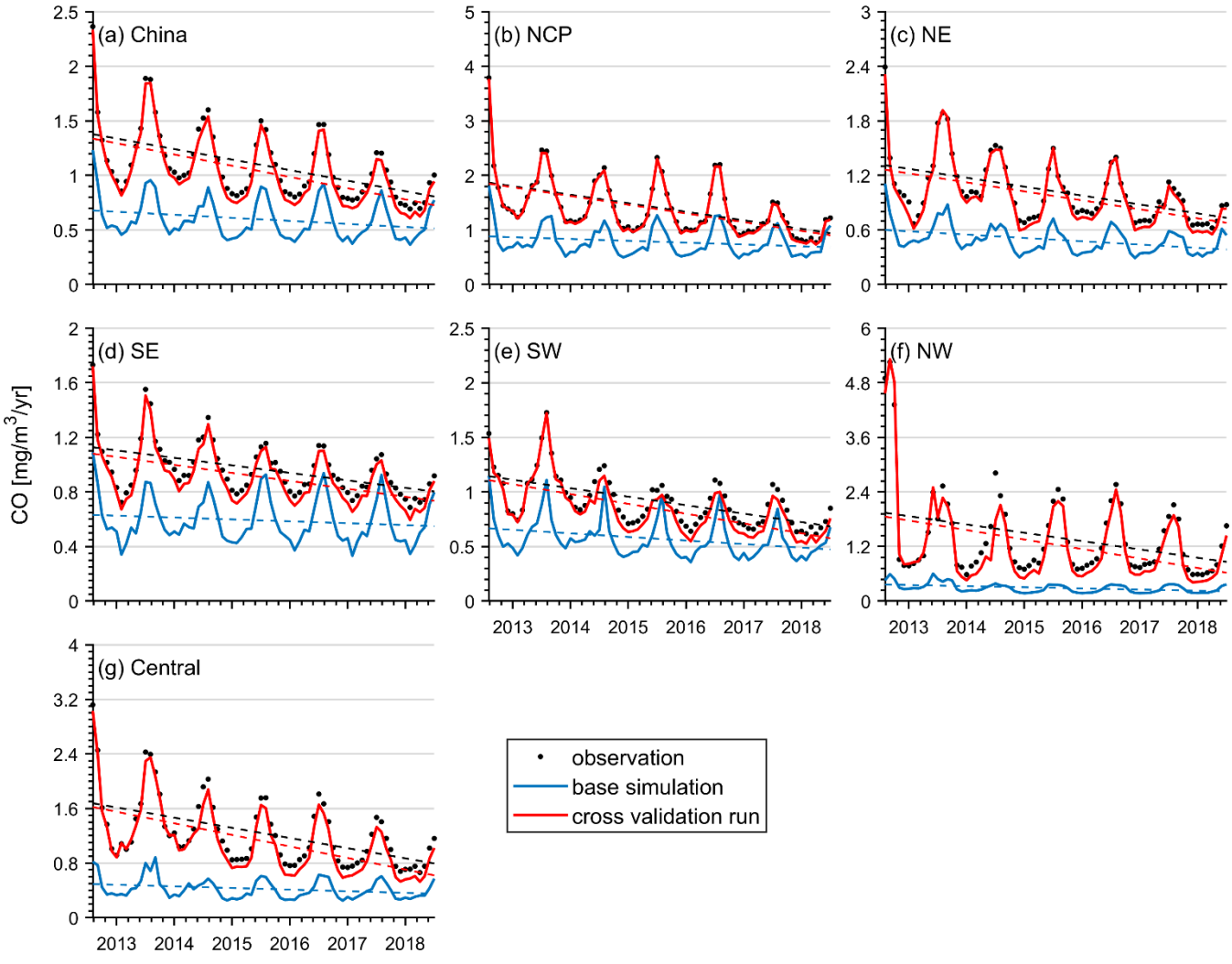

Figure 10: Same as Fig. 5 but for CO concentrations.

https://doi.org/10.5194/essd-2020-100
Preprint. Discussion started: 2 June 2020

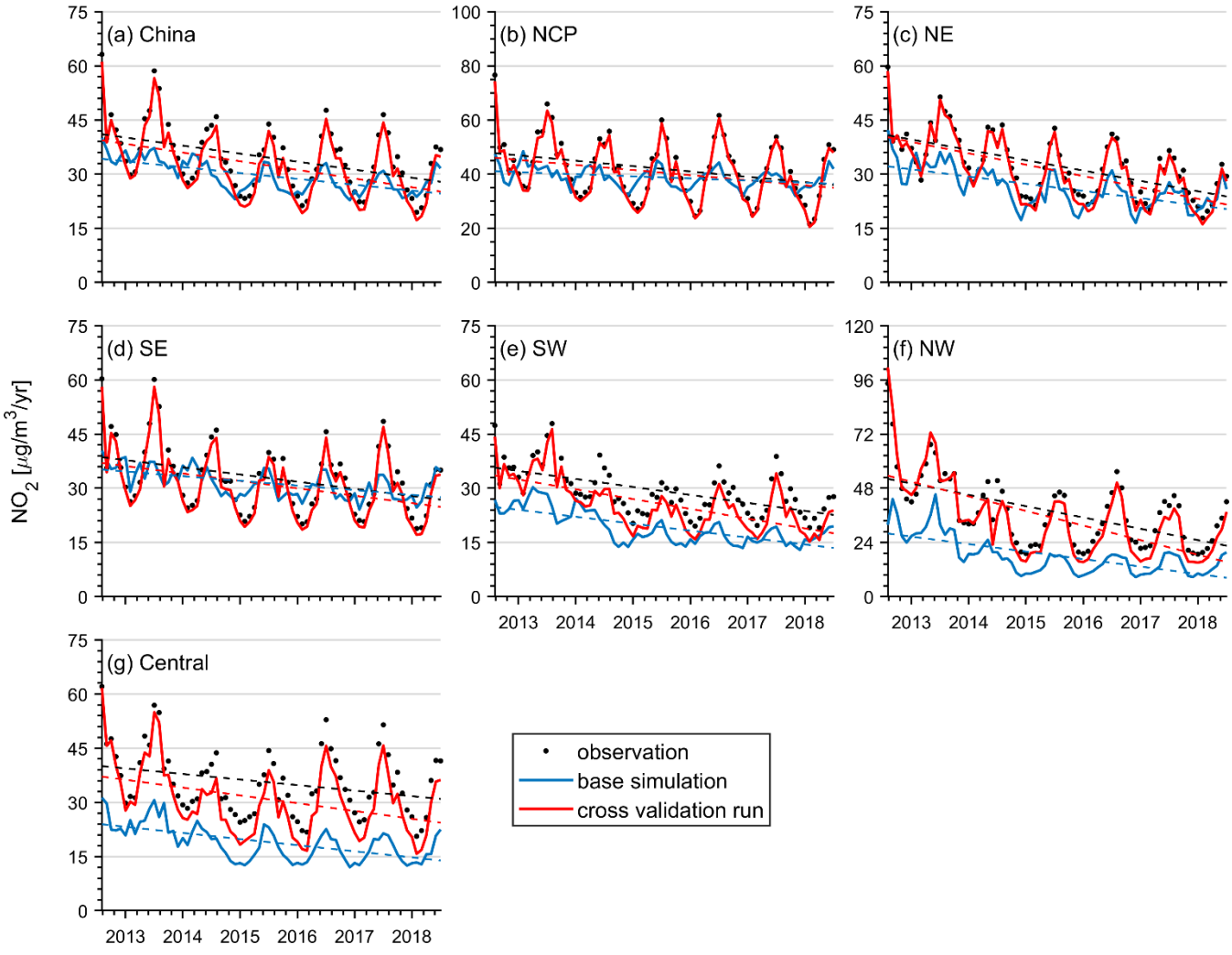

Figure 11: Same as Fig. 5 but for NO_2 concentrations.

https://doi.org/10.5194/essd-2020-100
Preprint. Discussion started: 2 June 2020

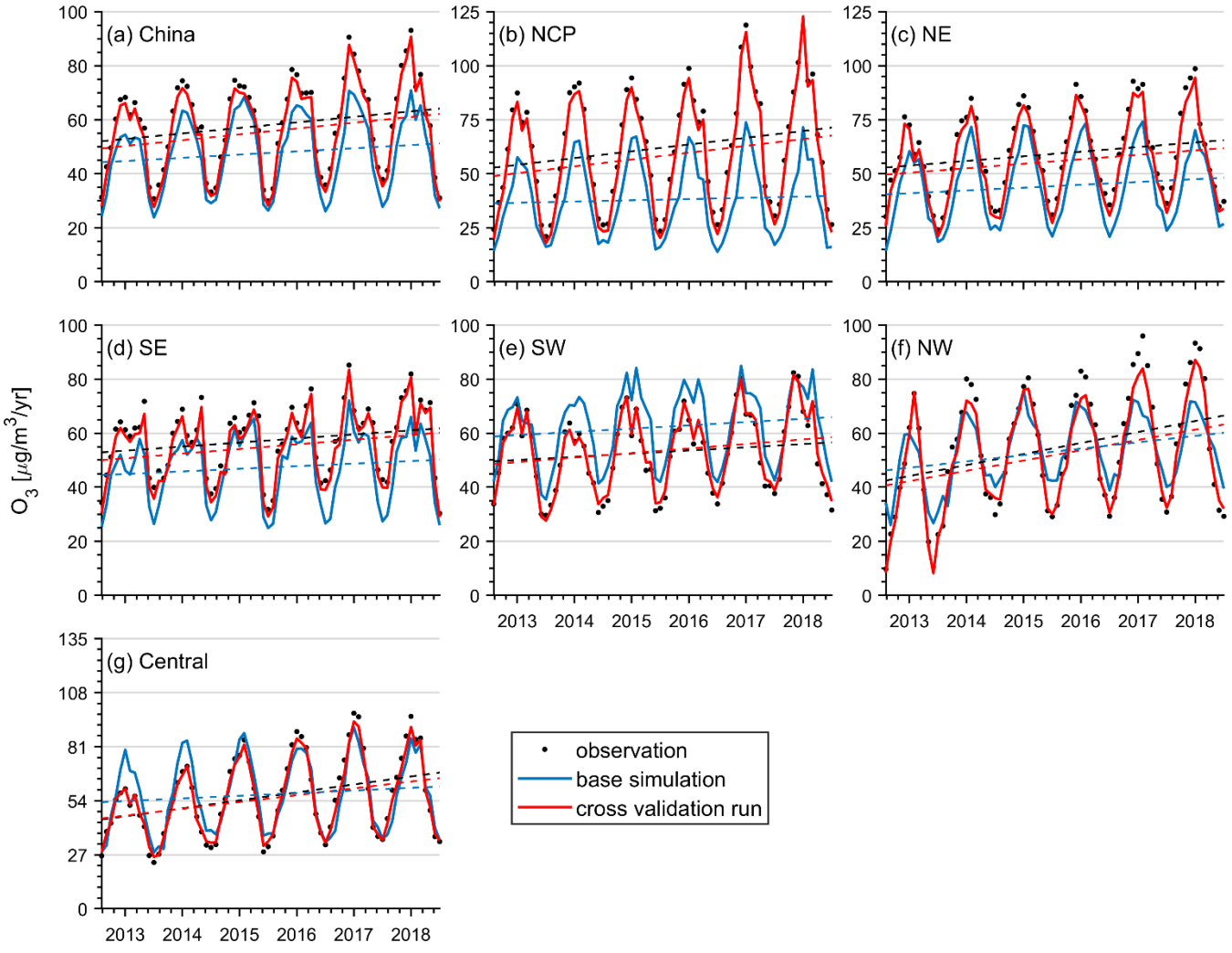

Figure 12: Same as Fig. 5 but for O_3 concentrations.

https://doi.org/10.5194/essd-2020-100
Preprint. Discussion started: 2 June 2020

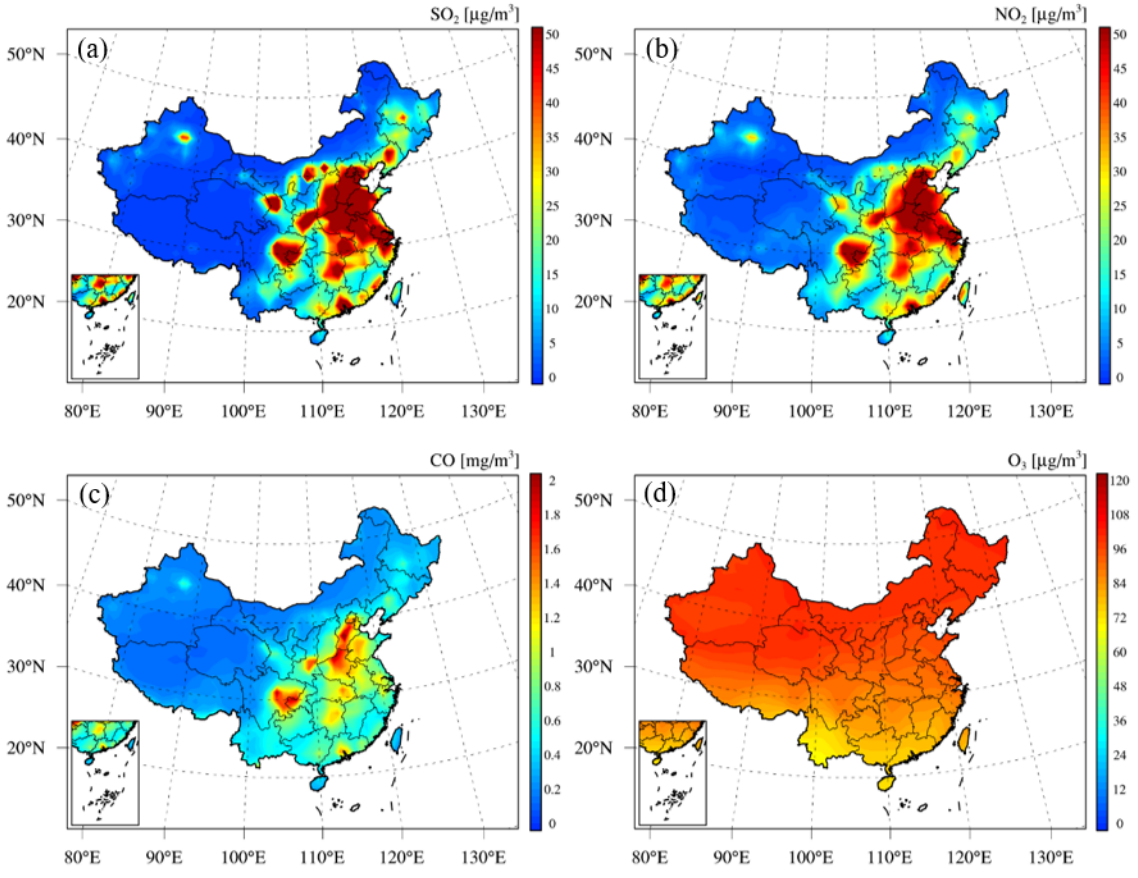

Figure 13: Spatial distributions of multi-year averaged concentrations of (a) SO_2, (b) NO_2, (c) CO and (d) O_3 from 2013 to 2018 obtained from CAMSRA.

https://doi.org/10.5194/essd-2020-100
Preprint. Discussion started: 2 June 2020

References

Athanasopoulou, E., Tombrou, M., Pandis, S. N., and Russell, A. G.: The role of sea-salt emissions and heterogeneous chemistry in the air quality of polluted coastal areas, Atmos. Chem. Phys., 8, 5755-5769, https://doi.org/10.5194/acp-8-5755-2008, 2008.

Barnes, W. L., Pagano, T. S., and Salomonson, V. V.: Prelaunch characteristics of the Moderate Resolution Imaging Spectroradiometer (MODIS) on EOS-AM1, IEEE Trans. Geosci. Remote Sensing, 36, 1088-1100, https://doi.org/10.1109/36.700993, 1998.

Bishop, C. H. and Toth, Z.: Ensemble transformation and adaptive observations, J. Atmos. Sci., 56, 1748-1765, https://doi.org/10.1175/1520-0469(1999)056<1748:ETAAO>2.0.CO;2, 1999.

Brasseur, G. P., Hauglustaine, D. A., Walters, S., Rasch, P. J., Muller, J. F., Granier, C., and Tie, X. X.: MOZART, a global chemical transport model for ozone and related chemical tracers 1. Model description, J. Geophys. Res.-Atmos., 103, 28265-28289, https://doi.org/10.1029/98jd02397, 1998.

Candiani, G., Carnevale, C., Finzi, G., Pisoni, E., and Volta, M.: A comparison of reanalysis techniques: Applying optimal interpolation and Ensemble Kalman Filtering to improve air quality monitoring at mesoscale, Sci. Total Environ., 458, 7-14, https://doi.org/10.1016/j.scitotenv.2013.03.089, 2013.

Carmichael, G., Sakurai, T., Streets, D., Hozumi, Y., Ueda, H., Park, S., Fung, C., Han, Z., Kajino, M., and Engardt, M.: MICS-Asia II: The model intercomparison study for Asia Phase II methodology and overview of findings, Atmos. Environ., 42, 3468-3490, https://doi.org/10.1016/j.atmosenv.2007.04.007, 2008.

Chen, G. B., Li, S. S., Knibbs, L. D., Hamm, N. A. S., Cao, W., Li, T. T., Guo, J. P., Ren, H. Y., Abramson, M. J., and Guo, Y. M.: A machine learning method to estimate PM2.5 concentrations across China with remote sensing, meteorological and land use information, Sci. Total Environ., 636, 52-60, https://doi.org/10.1016/j.scitotenv.2018.04.251, 2018.

Chen, Z. Y., Zhang, T. H., Zhang, R., Zhu, Z. M., Yang, J., Chen, P. Y., Ou, C. Q., and Guo, Y. M.: Extreme gradient boosting model to estimate PM2.5 concentrations with missing-filled satellite data in China, Atmos. Environ., 202, 180-189, https://doi.org/10.1016/j.atmosenv.2019.01.027, 2019.

Chu, Y. Y., Liu, Y. S., Li, X. Y., Liu, Z. Y., Lu, H. S., Lu, Y. A., Mao, Z. F., Chen, X., Li, N., Ren, M., Liu, F. F., Tian, L. Q., Zhu, Z. M., and Xiang, H.: A Review on Predicting Ground $PM_{2.5}$ Concentration Using Satellite Aerosol Optical Depth, Atmosphere, 7, 25, https://doi.org/ 10.3390/atmos7100129, 2016.

Cohen, A. J., Brauer, M., Burnett, R., Anderson, H. R., Frostad, J., Estep, K., Balakrishnan, K., Brunekreef, B., Dandona, L., Dandona, R., Feigin, V., Freedman, G., Hubbell, B., Jobling, A., Kan, H., Knibbs, L., Liu, Y., Martin, R., Morawska, L., Pope, C. A., Shin, H., Straif, K., Shaddick, G., Thomas, M., van Dingenen, R., van Donkelaar, A., Vos, T., Murray, C. J. L., and Forouzanfar, M. H.: Estimates and 25-year trends of the global burden of disease attributable to ambient air pollution: an analysis of data from the Global Burden of Diseases Study 2015, Lancet, 389, 1907-1918, https://doi.org/10.1016/s0140-6736(17)30505-6, 2017.

Dee, D. P., Uppala, S. M., Simmons, A. J., Berrisford, P., Poli, P., Kobayashi, S., Andrae, U., Balmaseda, M. A., Balsamo, G., Bauer, P., Bechtold, P., Beljaars, A. C. M., van de Berg, L., Bidlot, J., Bormann, N., Delsol, C., Dragani, R., Fuentes, M., Geer, A. J., Haimberger, L., Healy, S. B., Hersbach, H., Holm, E. V., Isaksen, L., Kallberg, P., Kohler, M., Matricardi, M., McNally, A. P., Monge-Sanz, B. M., Morcrette, J. J., Park, B. K., Peubey, C., de Rosnay, P., Tavolato, C., Thepaut, J. N., and Vitart, F.: The ERA-Interim reanalysis: configuration and performance of the data assimilation system, Q. J. R. Meteorol. Soc., 137, 553-597, https://doi.org/10.1002/qj.828, 2011.

https://doi.org/10.5194/essd-2020-100
Preprint. Discussion started: 2 June 2020

Deeter, M. N., Emmons, L. K., Francis, G. L., Edwards, D. P., Gille, J. C., Warner, J. X., Khattatov, B., Ziskin, D., Lamarque, J. F., Ho, S. P., Yudin, V., Attie, J. L., Packman, D., Chen, J., Mao, D., and Drummond, J. R.: Operational carbon monoxide retrieval algorithm and selected results for the MOPITT instrument, J. Geophys. Res.-Atmos., 108, 4399, https://doi.org/10.1029/2002JD003186, 2003.

Elbern, H., Strunk, A., Schmidt, H., and Talagrand, O.: Emission rate and chemical state estimation by 4-dimensional variational inversion, Atmos. Chem. Phys., 7, 3749-3769, https://doi.org/10.5194/acp-7-3749-2007, 2007.

Evensen, G.: Sequential data assimilation with a nonlinear quasi-geostrophic model using Monte Carlo methods to forecast error statistics, J. Geophys. Res.-Oceans, 99, 10143-10162, https://doi.org/10.1029/94JC00572, 1994.

Flemming, J., Benedetti, A., Inness, A., Engelen, R. J., Jones, L., Huijnen, V., Remy, S., Parrington, M., Suttie, M., Bozzo, A., Peuch, V. H., Akritidis, D., and Katragkou, E.: The CAMS interim Reanalysis of Carbon Monoxide, Ozone and Aerosol for 2003–2015, Atmos. Chem. Phys., 17, 1945-1983, https://doi.org/10.5194/acp-17-1945-2017, 2017.

Gaubert, B., Arellano, A. F., Barre, J., Worden, H. M., Emmons, L. K., Tilmes, S., Buchholz, R. R., Vitt, F., Raeder, K., Collins, N., Anderson, J. L., Wiedinmyer, C., Alonso, S. M., Edwards, D. P., Andreae, M. O., Hannigan, J. W., Petri, C., Strong, K., and Jones, N.: Toward a chemical reanalysis in a coupled chemistry-climate model: An evaluation of MOPITT CO assimilation and its impact on tropospheric composition, J. Geophys. Res.-Atmos., 121, 7310-7343, https://doi.org/10.1002/2016jd024863, 2016.

Granier, C., Lamarque, J., Mieville, A., Muller, J., Olivier, J., Orlando, J., Peters, J., Petron, G., Tyndall, G., and Wallens, S.: POET, a database of surface emissions of ozone precursors. 2005.

Hanna, S. R., Chang, J. C., and Fernau, M. E.: Monte Carlo estimates of uncertainties in predictions by a photochemical grid model (UAM-IV) due to uncertainties in input variables, Atmos. Environ., 32, 3619-3628, https://doi.org/10.1016/s1352-2310(97)00419-6, 1998.

Hauglustaine, D. A., Brasseur, G. P., Walters, S., Rasch, P. J., Muller, J. F., Emmons, L. K., and Carroll, C. A.: MOZART, a global chemical transport model for ozone and related chemical tracers 2. Model results and evaluation, J. Geophys. Res.-Atmos., 103, 28291-28335, https://doi.org/10.1029/98jd02398, 1998.

Hunt, B. R., Kostelich, E. J., and Szunyogh, I.: Efficient data assimilation for spatiotemporal chaos: A local ensemble transform Kalman filter, Physica D, 230, 112-126, https://doi.org/10.1016/j.physd.2006.11.008, 2007.

Inness, A., Ades, M., Agusti-Panareda, A., Barre, J., Benedictow, A., Blechschmidt, A. M., Dominguez, J. J., Engelen, R., Eskes, H., Flemming, J., Huijnen, V., Jones, L., Kipling, Z., Massart, S., Parrington, M., Pench, V. H., Razinger, M., Remy, S., Schulz, M., and Suttie, M.: The CAMS reanalysis of atmospheric composition, Atmos. Chem. Phys., 19, 3515-3556, https://doi.org/10.5194/acp-2018-1078, 2019.

Inness, A., Baier, F., Benedetti, A., Bouarar, I., Chabrillat, S., Clark, H., Clerbaux, C., Coheur, P., Engelen, R. J., Errera, Q., Flemming, J., George, M., Granier, C., Hadji-Lazaro, J., Huijnen, V., Hurtmans, D., Jones, L., Kaiser, J. W., Kapsomenakis, J., Lefever, K., Leitao, J., Razinger, M., Richter, A., Schultz, M. G., Simmons, A. J., Suttie, M., Stein, O., Thepaut, J. N., Thouret, V., Vrekoussis, M., Zerefos, C., and Team, M.: The MACC reanalysis: an 8 yr data set of atmospheric composition, Atmos. Chem. Phys., 13, 4073-4109, https://doi.org/10.5194/acp-13-4073-2013, 2013.

Janssens-Maenhout, G., Crippa, M., Guizzardi, D., Dentener, F., Muntean, M., Pouliot, G., Keating, T., Zhang, Q., Kurokawa, J., Wankmuller, R., van der Gon, H. D., Kuenen, J. J. P., Klimont, Z., Frost, G., Darras, S., Koffi, B., and Li, M.: HTAP_v2.2: a mosaic of regional and global emission grid maps for 2008 and 2010 to study hemispheric transport of air pollution, Atmos. Chem. Phys., 15, 11411-11432, https://doi.org/10.5194/acp-15-11411-2015, 2015.

Kan, H., Chen, R., and Tong, S.: Ambient air pollution, climate change, and population health in China, Environ. Int., 42, 10-19, https://doi.org/10.1016/j.envint.2011.03.003, 2012.

https://doi.org/10.5194/essd-2020-100
Preprint. Discussion started: 2 June 2020

Kobayashi, S., Ota, Y., Harada, Y., Ebita, A., Moriya, M., Onoda, H., Onogi, K., Kamahori, H., Kobayashi, C., Endo, H., Miyaoka, K., and Takahashi, K.: The JRA-55 Reanalysis: General Specifications and Basic Characteristics, J. Meteorol. Soc. Jpn., 93, 5-48, https://doi.org/10.2151/jmsj.2015-001, 2015.

Kong, L., Tang, X., Zhu, J., Wang, Z., Fu, J. S., Wang, X., Itahashi, S., Yamaji, K., Nagashima, T., Lee, H. J., Kim, C. H., Lin, C. Y., Chen, L., Zhang, M., Tao, Z., Li, J., Kajino, M., Liao, H., Wang, Z., Sudo, K., Wang, Y., Pan, Y., Tang, G., Li, M., Wu, Q., Ge, B., and Carmichael, G. R.: Evaluation and uncertainty investigation of the NO_2, CO and NH_3 modeling over China under the framework of MICS-Asia III, Atmos. Chem. Phys., 20, 181-202, https://doi.org/10.5194/acp-2018-1158, 2020.

Kumar, U., De Ridder, K., Lefebvre, W., and Janssen, S.: Data assimilation of surface air pollutants (O_3 and NO_2) in the regional-scale air quality model AURORA, Atmos. Environ., 60, 99-108, https://doi.org/10.1016/j.atmosenv.2012.06.005, 2012.

Levelt, P. F., Van den Oord, G. H. J., Dobber, M. R., Malkki, A., Visser, H., de Vries, J., Stammes, P., Lundell, J. O. V., and Saari, H.: The Ozone Monitoring Instrument, IEEE Trans. Geosci. Remote Sensing, 44, 1093-1101, https://doi.org/10.1109/TGRS.2006.872333, 2006.

Li, F., Tang, X., Wang, Z., Zhu, L., Wang, X., Wu, H., Lu, M., Li, J., and Zhu, J.: Estimation of Representative Errors of Surface Observations of Air Pollutant Concentrations Based on High-Density Observation Network over Beijing-Tianjin-Hebei Region, Chinese Journal of Atmospheric Sciences, 43, 277-284, https://doi.org/1006-9895(2019)43:2<277:>2.0.TX;2-S, 2019.

Li, J., Dong, H. B., Zeng, L. M., Zhang, Y. H., Shao, M., Wang, Z. F., Sun, Y. L., and Fu, P. Q.: Exploring Possible Missing Sinks of Nitrate and Its Precursors in Current Air Quality Models-A Case Simulation in the Pearl River Delta, China, Using an Observation-Based Box Model, Sola, 11, 124-128, https://doi.org/10.2151/sola.2015-029, 2015.

Li, J., Wang, Z., Wang, X., Yamaji, K., Takigawa, M., Kanaya, Y., Pochanart, P., Liu, Y., Irie, H., Hu, B., Tanimoto, H., and Akimoto, H.: Impacts of aerosols on summertime tropospheric photolysis frequencies and photochemistry over Central Eastern China, Atmos. Environ., 45, 1817-1829, https://doi.org/10.1016/j.atmosenv.2011.01.016, 2011.

Li, J., Wang, Z., Zhuang, G., Luo, G., Sun, Y., and Wang, Q.: Mixing of Asian mineral dust with anthropogenic pollutants over East Asia: a model case study of a super-duststorm in March 2010, Atmos. Chem. Phys., 12, 7591-7607, https://doi.org/10.1016/j.atmosenv.2011.01.016, 2012.

Li, K., Jacob, D. J., Liao, H., Shen, L., Zhang, Q., and Bates, K. H.: Anthropogenic drivers of 2013-2017 trends in summer surface ozone in China, Proc. Natl. Acad. Sci. U.S.A., 116, 422-427, https://doi.org/10.1073/pnas.1812168116, 2019.

Li, M., Liu, H., Geng, G. N., Hong, C. P., Liu, F., Song, Y., Tong, D., Zheng, B., Cui, H. Y., Man, H. Y., Zhang, Q., and He, K. B.: Anthropogenic emission inventories in China: a review, Natl. Sci. Rev., 4, 834-866, https://doi.org/10.1093/nsr/nwx150, 2017.

Li, T. W., Shen, H. F., Yuan, Q. Q., Zhang, X. C., and Zhang, L. P.: Estimating Ground-Level $PM_{2.5}$ by Fusing Satellite and Station Observations: A Geo-Intelligent Deep Learning Approach, Geophys. Res. Lett., 44, 11985-11993, https://doi.org/10.1002/2017gl075710, 2017.

Liang, X., Zheng, X. G., Zhang, S. P., Wu, G. C., Dai, Y. J., and Li, Y.: Maximum likelihood estimation of inflation factors on error covariance matrices for ensemble Kalman filter assimilation, Q. J. R. Meteorol. Soc., 138, 263-273, https://doi.org/10.1002/qj.912, 2012.

Lin, C. Q., Li, Y., Yuan, Z. B., Lau, A. K. H., Li, C. C., and Fung, J. C. H.: Using satellite remote sensing data to estimate the high-resolution distribution of ground-level $PM_{2.5}$, Remote Sens. Environ., 156, 117-128, https://doi.org/10.1016/j.rse.2014.09.015, 2015.

Lin, C. Q., Liu, G., Lau, A. K. H., Li, Y., Li, C. C., Fung, J. C. H., and Lao, X. Q.: High-resolution satellite remote sensing of provincial PM2.5 trends in China from 2001 to 2015, Atmos. Environ., 180, 110-116, https://doi.org/10.1016/j.atmosenv.2018.02.045, 2018.

https://doi.org/10.5194/essd-2020-100
Preprint. Discussion started: 2 June 2020

Liu, J. J., Weng, F. Z., and Li, Z. Q.: Satellite-based $PM_{2.5}$ estimation directly from reflectance at the top of the atmosphere using a machine learning algorithm, Atmos. Environ., 208, 113-122, https://doi.org/10.1016/j.atmosenv.2019.04.002, 2019.

Lu, M. M., Tang, X., Wang, Z. F., Gbaguidi, A., Liang, S. W., Hu, K., Wu, L., Wu, H. J., Huang, Z., and Shen, L. J.: Source tagging modeling study of heavy haze episodes under complex regional transport processes over Wuhan megacity, Central China, Environ. Pollut., 231, 612-621, https://doi.org/10.1016/j.envpol.2017.08.046, 2017.

Lu, Z., Streets, D. G., Zhang, Q., Wang, S., Carmichael, G. R., Cheng, Y. F., Wei, C., Chin, M., Diehl, T., and Tan, Q.: Sulfur dioxide emissions in China and sulfur trends in East Asia since 2000, Atmos. Chem. Phys., 10, 6311-6331, https://doi.org/10.5194/acp-10-6311-2010, 2010.

Ma, Z. W., Hu, X. F., Huang, L., Bi, J., and Liu, Y.: Estimating Ground-Level $PM_{2.5}$ in China Using Satellite Remote Sensing, Environ. Sci. Technol., 48, 7436-7444, https://doi.org/10.1021/es5009399, 2014.

Ma, Z. W., Hu, X. F., Sayer, A. M., Levy, R., Zhang, Q., Xue, Y. G., Tong, S. L., Bi, J., Huang, L., and Liu, Y.: Satellite-Based Spatiotemporal Trends in PM2.5 Concentrations: China, 2004-2013, Environ. Health Perspect., 124, 184-192, https://doi.org/10.1289/ehp.1409481, 2016.

Miyazaki, K., Eskes, H. J., and Sudo, K.: A tropospheric chemistry reanalysis for the years 2005–2012 based on an assimilation of OMI, MLS, TES, and MOPITT satellite data, Atmos. Chem. Phys., 15, 8315-8348, https://doi.org/10.5194/acp-15-8315-2015, 2015.

Miyazaki, K., Bowman, K., Sekiya, T., Eskes, H., Boersma, F., Worden, H., Livesey, N., Payne, V. H., Sudo, K., Kanaya, Y., Takigawa, M., and Ogochi, K.: An updated tropospheric chemistry reanalysis and emission estimates, TCR-2, for 2005–2018, Earth Syst. Sci. Data Discuss., https://doi.org/10.5194/essd-2020-30, in review, 2020.

NBSC, China energy statistical Yearbook, 2017a, http://tongji.cnki.net/kns55/Navi/HomePage.aspx?id=N2017110016&name=YCXME&floor=1, Accessed date: 17 April 2020.

NBSC, China statistical Yearbook on environment, 2017b, http://www.stats.gov.cn/ztjc/ztsj/hjtjzl/, Accessed date: 17 April 2020.

Nenes, A., Pandis, S. N., and Pilinis, C.: ISORROPIA: A new thermodynamic equilibrium model for multiphase multicomponent inorganic aerosols, Aquat. Geochem., 4, 123-152, https://doi.org/10.1023/a:1009604003981, 1998.

Ott, E., Hunt, B. R., Szunyogh, I., Zimin, A. V., Kostelich, E. J., Corazza, M., Kalnay, E., Patil, D. J., and Yorke, J. A.: A local ensemble Kalman filter for atmospheric data assimilation, Tellus Ser. A-Dyn. Meteorol. Oceanol., 56, 415-428, https://doi.org/10.1111/j.1600-0870.2004.00076.x, 2004.

Price, C., Penner, J., and Prather, M.: NO_x from lightning .1. Global distribution based on lightning physics, J. Geophys. Res.-Atmos., 102, 5929-5941, https://doi.org/10.1029/96jd03504, 1997.

Qi, J., Zheng, B., Li, M., Yu, F., Chen, C. C., Liu, F., Zhou, X. F., Yuan, J., Zhang, Q., and He, K. B.: A high-resolution air pollutants emission inventory in 2013 for the Beijing-Tianjin-Hebei region, China, Atmos. Environ., 170, 156-168, https://doi.org/10.1016/j.atmosenv.2017.09.039, 2017.

Randerson, J. T., Van Der Werf, G. R., Giglio, L., Collatz, G. J., and Kasibhatla, P. S.: Global Fire Emissions Database, Version 4.1 (GFEDv4). ORNL Distributed Active Archive Center, 2017.

Randles, C. A., da Silva, A. M., Buchard, V., Colarco, P. R., Darmenov, A., Govindaraju, R., Smirnov, A., Holben, B., Ferrare, R., Hair, J., Shinozuka, Y., and Flynn, C. J.: The MERRA-2 Aerosol Reanalysis, 1980 Onward. Part I: System Description and Data Assimilation Evaluation, J. Clim., 30, 6823-6850, https://doi.org/10.1175/jcli-d-16-0609.1, 2017.

Rienecker, M. M., Suarez, M. J., Gelaro, R., Todling, R., Bacmeister, J., Liu, E., Bosilovich, M. G., Schubert, S. D., Takacs, L., Kim, G. K., Bloom, S., Chen, J. Y., Collins, D., Conaty, A., Da Silva, A., Gu, W., Joiner, J., Koster, R. D., Lucchesi, R., Molod, A., Owens, T.,

https://doi.org/10.5194/essd-2020-100
Preprint. Discussion started: 2 June 2020

Pawson, S., Pegion, P., Redder, C. R., Reichle, R., Robertson, F. R., Ruddick, A. G., Sienkiewicz, M., and Woollen, J.: MERRA: NASA's Modern-Era Retrospective Analysis for Research and Applications, J. Clim., 24, 3624-3648, https://doi.org/10.1175/jcli-d-11-00015.1, 2011.

Saha, S., Moorthi, S., Pan, H. L., Wu, X. R., Wang, J. D., Nadiga, S., Tripp, P., Kistler, R., Woollen, J., Behringer, D., Liu, H. X., Stokes, D., Grumbine, R., Gayno, G., Wang, J., Hou, Y. T., Chuang, H. Y., Juang, H. M. H., Sela, J., Iredell, M., Treadon, R., Kleist, D., Van Delst, P., Keyser, D., Derber, J., Ek, M., Meng, J., Wei, H. L., Yang, R. Q., Lord, S., Van den Dool, H., Kumar, A., Wang, W. Q., Long, C., Chelliah, M., Xue, Y., Huang, B. Y., Schemm, J. K., Ebisuzaki, W., Lin, R., Xie, P. P., Chen, M. Y., Zhou, S. T., Higgins, W., Zou, C. Z., Liu, Q. H., Chen, Y., Han, Y., Cucurull, L., Reynolds, R. W., Rutledge, G., and Goldberg, M.: THE NCEP CLIMATE FORECAST SYSTEM REANALYSIS, Bulletin of the American Meteorological Society, 91, 1015-1057, https://doi.org/10.1175/2010BAMS3001.1, 2010.

Sakov, P. and Bertino, L.: Relation between two common localisation methods for the EnKF, Comput. Geosci., 15, 225-237, https://doi.org/10.1007/s10596-010-9202-6, 2011.

Shin, M., Kang, Y., Park, S., Im, J., Yoo, C., and Quackenbush, L. J.: Estimating ground-level particulate matter concentrations using satellite-based data: a review, GISci. Remote Sens., https://doi.org/10.1080/15481603.2019.1703288, 2019. 1-16, 2019.

Silver, B., Reddington, C. L., Arnold, S. R., and Spracklen, D. V.: Substantial changes in air pollution across China during 2015-2017, Environ. Res. Lett., 13, 8, https://doi.org/10.1088/1748-9326/aae718, 2018.

Sindelarova, K., Granier, C., Bouarar, I., Guenther, A., Tilmes, S., Stavrakou, T., Muller, J. F., Kuhn, U., Stefani, P., and Knorr, W.: Global data set of biogenic VOC emissions calculated by the MEGAN model over the last 30 years, Atmos. Chem. Phys., 14, 9317-9341, https://doi.org/10.5194/acp-14-9317-2014, 2014.

Skamarock, W. C.: A description of the advanced research WRF version 3, Ncar Technical, 113, 7--25, 2008.

Streets, D. G., Bond, T. C., Carmichael, G. R., Fernandes, S. D., Fu, Q., He, D., Klimont, Z., Nelson, S. M., Tsai, N. Y., Wang, M. Q., Woo, J. H., and Yarber, K. F.: An inventory of gaseous and primary aerosol emissions in Asia in the year 2000, J. Geophys. Res.-Atmos., 108, 23, https://doi.org/10.1029/2002jd003093, 2003.

Tang, X., Zhu, J., Wang, Z. F., and Gbaguidi, A.: Improvement of ozone forecast over Beijing based on ensemble Kalman filter with simultaneous adjustment of initial conditions and emissions, Atmos. Chem. Phys., 11, 12901-12916, https://doi.org/10.5194/acp-11-12901-2011, 2011.

Tang, X., Zhu, J., Wang, Z. F., Wang, M., Gbaguidi, A., Li, J., Shao, M., Tang, G. Q., and Ji, D. S.: Inversion of CO emissions over Beijing and its surrounding areas with ensemble Kalman filter, Atmos. Environ., 81, 676-686, https://doi.org/10.1016/j.atmosenv.2013.08.051, 2013.

Tang, X., Kong, L., Zhu, J., Wang, Z. F. , Li, J. J., Wu, H. J., Wu, Q. Z., Chen, H. S., Zhu, L. L., Wang, W., Liu, B., Wang, Q., Chen D. H., Pan Y. P., Song, T., Li, F., Zheng, H. T., Jia, G. L., Lu, M. M., Wu, L., Carmichael, G. R.: A Six-year long High-resolution Air Quality Reanalysis Dataset over China from 2013 to 2018. V2. Science Data Bank, https://doi.org/10.11922/sciencedb.00053, 2020a.

Tang, X., Kong, L., Zhu, J., Wang, Z. F. , Li, J. J., Wu, H. J., Wu, Q. Z., Chen, H. S., Zhu, L. L., Wang, W., Liu, B., Wang, Q., Chen D. H., Pan Y. P., Song, T., Li, F., Zheng, H. T., Jia, G. L., Lu, M. M., Wu, L., Carmichael, G. R.: A Six-year long High-resolution Air Quality Reanalysis Dataset over China from 2013 to 2018 (monthly and annual version). V1. Science Data Bank, https://doi.org/10.11922/sciencedb.00092, 2020b.

van der A, R. J., Allaart, M. A. F., and Eskes, H. J.: Extended and refined multi sensor reanalysis of total ozone for the period 1970-2012, Atmos. Meas. Tech., 8, 3021-3035, https://doi.org/10.5194/amt-8-3021-2015, 2015.

https://doi.org/10.5194/essd-2020-100
Preprint. Discussion started: 2 June 2020

van der Werf, G. R., Randerson, J. T., Giglio, L., Collatz, G. J., Mu, M., Kasibhatla, P. S., Morton, D. C., DeFries, R. S., Jin, Y., and van Leeuwen, T. T.: Global fire emissions and the contribution of deforestation, savanna, forest, agricultural, and peat fires (1997–2009), Atmos. Chem. Phys., 10, 11707-11735, https://doi.org/10.5194/acp-10-11707-2010, 2010.

van Donkelaar, A., Martin, R. V., Brauer, M., Hsu, N. C., Kahn, R. A., Levy, R. C., Lyapustin, A., Sayer, A. M., and Winker, D. M.: Global Estimates of Fine Particulate Matter using a Combined Geophysical-Statistical Method with Information from Satellites, Models, and Monitors, Environ. Sci. Technol., 50, 3762-3772, https://doi.org/10.1021/acs.est.5b05833, 2016.

van Donkelaar, A., Martin, R. V., Brauer, M., Kahn, R., Levy, R., Verduzco, C., and Villeneuve, P. J.: Global Estimates of Ambient Fine Particulate Matter Concentrations from Satellite-Based Aerosol Optical Depth: Development and Application, Environ. Health Perspect., 118, 847-855, https://doi.org/10.1289/ehp.0901623, 2010.

von Schneidemesser, E., Monks, P. S., Allan, J. D., Bruhwiler, L., Forster, P., Fowler, D., Lauer, A., Morgan, W. T., Paasonen, P., Righi, M., Sindelarova, K., and Sutton, M. A.: Chemistry and the Linkages between Air Quality and Climate Change, Chem. Rev., 115, 3856-3897, https://doi.org/10.1021/acs.chemrev.5b00089, 2015.

Walcek, C. J. and Aleksic, N. M.: A simple but accurate mass conservative, peak-preserving, mixing ratio bounded advection algorithm with FORTRAN code, Atmos. Environ., 32, 3863-3880, https://doi.org/10.1016/S1352-2310(98)00099-5, 1998.

Wang, X. G. and Bishop, C. H.: A comparison of breeding and ensemble transform Kalman filter ensemble forecast schemes, J. Atmos. Sci., 60, 1140-1158, https://doi.org/10.1175/1520-0469(2003)060<1140:Acobae>2.0.Co;2, 2003.

Wang, Z. F., Sha, W. M., and Ueda, H.: Numerical modeling of pollutant transport and chemistry during a high-ozone event in northern Taiwan, Tellus Ser. B-Chem. Phys. Meteorol., 52, 1189-1205, https://doi.org/10.1034/j.1600-0889.2000.01064.x, 2000.

Wesely, M. L.: Parameterization of surface resistances to gaseous dry deposition in regional-scale numerical models, Atmos. Environ., 23, 1293-1304, https://doi.org/10.1016/0004-6981(89)90153-4 1989.

Wu, H. J., Tang, X., Wang, Z. F., Wu, L., Lu, M. M., Wei, L. F., and Zhu, J.: Probabilistic Automatic Outlier Detection for Surface Air Quality Measurements from the China National Environmental Monitoring Network, Adv. Atmos. Sci., 35, 1522-1532, https://doi.org/10.1007/s00376-018-8067-9, 2018.

Xue, T., Zheng, Y., Tong, D., Zheng, B., Li, X., Zhu, T., and Zhang, Q.: Spatiotemporal continuous estimates of PM2.5 concentrations in China, 2000–2016: A machine learning method with inputs from satellites, chemical transport model, and ground observations, Environ. Int., 123, 345-357, https://doi.org/10.1016/j.envint.2018.11.075, 2019.

Xue, T., Zheng, Y. X., Geng, G. N., Zheng, B., Jiang, X. J., Zhang, Q., and He, K. B.: Fusing Observational, Satellite Remote Sensing and Air Quality Model Simulated Data to Estimate Spatiotemporal Variations of $PM_{2.5}$ Exposure in China, Remote Sens., 9, 19, https://doi.org/10.3390/rs9030221, 2017.

Yan, X. Y., Akimoto, H., and Ohara, T.: Estimation of nitrous oxide, nitric oxide and ammonia emissions from croplands in East, Southeast and South Asia, Glob. Change Biol., 9, 1080-1096, https://doi.org/10.1046/j.1365-2486.2003.00649.x, 2003.

Yao, F., Wu, J., Li, W., and Peng, J.: A spatially structured adaptive two-stage model for retrieving ground-level $PM_{2.5}$ concentrations from VIIRS AOD in China, ISPRS Journal of Photogrammetry and Remote Sensing, 151, 263-276, https://doi.org/10.1016/j.isprsjprs.2019.03.011, 2019.

You, W., Zang, Z. L., Zhang, L. F., Li, Y., Pan, X. B., and Wang, W. Q.: National-Scale Estimates of Ground-Level $PM_{2.5}$ Concentration in China Using Geographically Weighted Regression Based on 3 km Resolution MODIS AOD, Remote Sens., 8, 13, https://doi.org/10.3390/rs8030184, 2016.

https://doi.org/10.5194/essd-2020-100
Preprint. Discussion started: 2 June 2020

Yumimoto, K., Tanaka, T. Y., Oshima, N., and Maki, T.: JRAero: the Japanese Reanalysis for Aerosol v1.0, Geosci. Model Dev., 10, 3225-3253, https://doi.org/10.5194/gmd-10-3225-2017, 2017.

Zaveri, R. A. and Peters, L. K.: A new lumped structure photochemical mechanism for large-scale applications, J. Geophys. Res.-Atmos., 104, 30387-30415, https://doi.org/10.1029/1999jd900876, 1999.

Zhan, Y., Luo, Y. Z., Deng, X. F., Chen, H. J., Grieneisen, M. L., Shen, X. Y., Zhu, L. Z., and Zhang, M. H.: Spatiotemporal prediction of continuous daily PM2.5 concentrations across China using a spatially explicit machine learning algorithm, Atmos. Environ., 155, 129-139, https://doi.org/10.1016/j.atmosenv.2017.02.023, 2017.

Zhan, Y., Luo, Y. Z., Deng, X. F., Zhang, K. S., Zhang, M. H., Grieneisen, M. L., and Di, B. F.: Satellite-Based Estimates of Daily NO2 Exposure in China Using Hybrid Random Forest and Spatiotemporal Kriging Model, Environ. Sci. Technol., 52, 4180-4189, https://doi.org/10.1021/acs.est.7b05669, 2018.

Zhang, H. Y., Di, B. F., Liu, D. R., Li, J. R., and Zhan, Y.: Spatiotemporal distributions of ambient SO_2 across China based on satellite retrievals and ground observations: Substantial decrease in human exposure during 2013-2016, Environ. Res., 179, 9, https://doi.org/10.1016/j.envres.2019.108795, 2019.

Zhang, Q., Streets, D. G., Carmichael, G. R., He, K. B., Huo, H., Kannari, A., Klimont, Z., Park, I. S., Reddy, S., Fu, J. S., Chen, D., Duan, L., Lei, Y., Wang, L. T., and Yao, Z. L.: Asian emissions in 2006 for the NASA INTEX-B mission, Atmos. Chem. Phys., 9, 5131-5153, https://doi.org/10.5194/acp-9-5131-2009, 2009.

Zheng, B., Chevallier, F., Ciais, P., Yin, Y., Deeter, M. N., Worden, H. M., Wang, Y. L., Zhang, Q., and He, K. B.: Rapid decline in carbon monoxide emissions and export from East Asia between years 2005 and 2016, Environ. Res. Lett., 13, 9, https://doi.org/10.1088/1748-9326/aab2b3, 2018a.

Zheng, B., Chevallier, F., Yin, Y., Ciais, P., Fortems-Cheiney, A., Deeter, M. N., Parker, R. J., Wang, Y. L., Worden, H. M., and Zhao, Y. H.: Global atmospheric carbon monoxide budget 2000-2017 inferred from multi-species atmospheric inversions, Earth Syst. Sci. Data, 11, 1411-1436, https://doi.org/10.5194/essd-11-1411-2019, 2019.

Zheng, B., Tong, D., Li, M., Liu, F., Hong, C. P., Geng, G. N., Li, H. Y., Li, X., Peng, L. Q., Qi, J., Yan, L., Zhang, Y. X., Zhao, H. Y., Zheng, Y. X., He, K. B., and Zhang, Q.: Trends in China's anthropogenic emissions since 2010 as the consequence of clean air actions, Atmos. Chem. Phys., 18, 14095-14111, https://doi.org/10.5194/acp-18-14095-2018, 2018b.

Zheng, Y. X., Xue, T., Zhang, Q., Geng, G. N., Tong, D., Li, X., and He, K. B.: Air quality improvements and health benefits from China's clean air action since 2013, Environ. Res. Lett., 12, 9, https://doi.org/10.1088/1748-9326/aa8a32, 2017.

Zou, B., Chen, J. W., Zhai, L., Fang, X., and Zheng, Z.: Satellite Based Mapping of Ground $PM_{2.5}$ Concentration Using Generalized Additive Modeling, Remote Sens., 9, 16, https://doi.org/10.3390/rs9010001, 2017.